Killer cell Immunoglobulin-like Receptor 3DL1 polymorphism defines distinct hierarchies of HLA class I recognition

Philippa M. Saunders[1]*, Phillip Pymm[2,3]*, Gabriella Pietra[4,5], Victoria A. Hughes[2,3], Corinne Hitchen[2], Geraldine M. O'Connor[1], Fabrizio Loiacono[6], Jacqueline Widjaja[1], David A. Price[7,8], Michela Falco[6], Maria C. Mingari[4,5], Lorenzo Moretta[9], Daniel W. McVicar[10], Jamie Rossjohn[2,3,7#], Andrew G. Brooks[1#] and Julian P. Vivian[2,3#]

[1]Department of Microbiology and Immunology, Peter Doherty Institute for Infection and Immunity, The University of Melbourne, Parkville, Victoria 3010, Australia

[2]Infection and Immunity Program & Department of Biochemistry and Molecular Biology, Biomedicine Discovery Institute, Monash University, Clayton, Victoria 3800, Australia

[3]Australian Research Council Centre of Excellence in Advanced Molecular Imaging, Monash University, Clayton, Victoria 3800, Australia

[4]Department of Experimental Medicine, University of Genova, Genoa, 16132 Italy

[5]IRCCS AOU San Martino-IST (National Institute for Cancer Research), Genoa, 16132 Italy

[6]IRCCS Istituto Giannina Gaslini, Genoa, Italy

[7]Institute of Infection and Immunity, Cardiff University School of Medicine, Heath Park, Cardiff CF14 4XN, UK

[8]Human Immunology Section, Vaccine Research Center, National Institute of Allergy and Infectious Diseases, National Institutes of Health, Bethesda, MD 20892, USA

[9]IRCCS Ospedale Pediatrico Bambino Gesù, Roma ITALY

[10] Cancer and Inflammation Program, National Cancer Institute-Frederick, Frederick, MD 21702, USA

* These authors contributed equally.

#Joint senior and corresponding authors. Address correspondence to Jamie Rossjohn, email: jamie.rossjohn@monash.edu, Andrew Brooks, email: agbrooks@unimelb.edu.au, or Julian Vivian, email: julian.vivian@monash.edu

Total character count: 37,391

Running title: KIR3DL1 polymorphism and HLA class I recognition

Non-standard abbreviations

AML	Acute Myeloid Leukaemia;
HLA-I	Human Leukocyte Antigen class I molecules
KIR	Killer cell Immunoglobulin-like Receptor
LF9	LSSPVTKSF
MFI	Mean Fluorescence Intensity

Abstract

NK cells play a key role in immunity, but how HLA-I and KIR3DL1 polymorphism impacts on disease outcome remains unclear. KIR3DL1 (*001/*005/*015) tetramers were screened for reactivity against a panel of HLA-I molecules. This revealed different and distinct hierarchies of specificity for each KIR3DL1 allotype, with KIR3DL1*005 recognising the widest array of HLA-I ligands. These differences were further reflected in functional studies utilising NK clones expressing these specific KIR3DL1 allotypes. Unexpectedly, the Ile/Thr80 dimorphism in the Bw4-motif did not categorically define strong/weak KIR3DL1 recognition. Although the KIR3DL1*001, *005 and *015 polymorphisms are remote from the KIR3DL1-HLA-I interface, the structures of these three KIR3DL1-HLA-I complexes showed that the broader HLA-I specificity of KIR3DL1*005 correlated with an altered KIR3DL1*005 interdomain positioning and increased mobility within its ligand-binding site. Collectively, we provide a generic framework for understanding the impact of KIR3DL1 polymorphism on the recognition of HLA-I allomorphs.

Caption: "Rossjohn, Brooks, Vivian and colleagues provide the most complete picture to date of the impact of KIR3DL1 polymorphism on HLA class I recognition, which can be used to both re-evaluate previous work on the involvement of KIR3DL1 in disease, as well as inform future disease association studies."

INTRODUCTION

Natural Killer (NK) cells play a key innate role in the elimination of infected or transformed cells that are no longer identified as self (Ljunggren and Karre, 1990). The interaction of inhibitory Killer cell Immunoglobulin-like receptors (KIR) with Human Leukocyte Antigen (HLA) class I molecules (HLA-I) is important during NK cell development and regulates NK cell lysis of target cells that have downregulated HLA-I expression or express different HLA-I allotypes. The highly polymorphic nature of both KIR and HLA-I has resulted in several studies linking the presence of particular KIR/HLA-I combinations with disease outcomes, in particular in the context of chronic viral infections. For example, the presence of *KIR3DL1* and certain *HLA-I* alleles has been associated with delayed progression to AIDS in HIV-infected individuals (Martin et al., 2007). Nevertheless the mechanistic basis for such associations remains unclear.

KIR3DL1 recognises HLA-I allotypes that bear the Bw4 motif, a region that spans residues 77-83 on the α1-helix of the HLA-I molecule. The crystal structure of the KIR3DL1*001-peptide-HLA-B*57:01 complex demonstrated that KIR3DL1 bound two regions that are highly conserved across HLA-I allotypes in addition to residues within the Bw4 motif. Here, the interaction is ultimately dependent upon the microarchitecture of the Bw4 motif and the sequence of the bound peptide (Gumperz et al., 1997; Gumperz et al., 1995; O'Connor et al., 2014; Saunders et al., 2015; Thananchai et al., 2007; Vivian et al., 2011). Additionally, there is evidence that polymorphism both within and outside the Bw4 motif can impact on KIR3DL1 recognition (Gumperz et al., 1995; O'Connor et al., 2014; Thananchai et al., 2007). For instance, HLA-A*32:01, HLA-B*51:01 and HLA-B*58:01 generally confer robust protection of target cells from lysis by KIR3DL1^{+} NK cells, while HLA-B*15:13 and HLA-B*27:05 have sometimes been associated with moderate or weak inhibitory effects, despite the fact that all these molecules are HLA-Bw4 allotypes (Carr et al., 2005; Cella et al., 1994; Gumperz et al., 1995; Litwin et al., 1994; Luque et al., 1996; Norman et al., 2009; O'Connor et al., 2007; Rojo et al., 1997).

Our understanding of the hierarchical HLA-Bw4 preferences of KIR3DL1 is further confounded by polymorphism within the *KIR3DL1* locus. More than 100 allelic variants of the *KIR3DL1* gene have been described, phylogenetically spanning three main lineages based on the sequence differences across the three extracellular domains (D0-D1-D2) of the KIR3DL1 molecule (Norman et al., 2009; Robinson et al., 2015). Namely, there are two diverse inhibitory lineages comprising *KIR3DL1*005*-like and **015*-like alleles, while the third lineage is much more constrained at a population level, and consists largely of the activating *KIR3DLS1*013* allele (Norman et al., 2007; Parham et al., 2012). *KIR3DL1* polymorphism was initially associated with differences in cell

surface expression with allotypes such as KIR3DL1*001, *002 and *008 being expressed at high levels, *005 and *009 at lower levels and *004 being largely retained intracellularly (Gardiner et al., 2001; Mulrooney et al., 2015; Pando et al., 2003; Taner et al., 2011). *KIR3DL1* polymorphism can also affect recognition of HLA-I with polymorphisms at positions including 238 and 283 impacting recognition of various HLA-Bw4 ligands (Carr et al., 2005; O'Connor et al., 2014; Thananchai et al., 2007; Yawata et al., 2006b). Similarly, recent evidence has shown enhanced recognition of HLA-B*44:03 by KIR3DL1*005 relative to KIR3DL1*001 and KIR3DL1*009 (Mulrooney et al., 2015). However, the molecular mechanisms underpinning these effects remain unclear.

Early studies correlated a subset of HLA-Bw4 allotypes possessing Ile at position 80 with elevated protection from lysis by NK cells, which led to the hypothesis that Ile80 marked "high affinity" ligands for KIR3DL1 and even KIR3DS1 (Cella et al., 1994; Martin et al., 2007). This concept has been used to frame subsequent studies examining disease progression. For example, in HIV-infected individuals, the presence of KIR3DL1 allotypes with high cell surface expression in combination with Ile80-encoding HLA-Bw4 allotypes was associated with reduced viral replication and delayed progression to AIDS (Martin et al., 2007). Similarly, the presence of both KIR3DL1 and HLA-Bw4 allotypes with Ile80 was associated with an increased risk of relapse after autologous haematopoietic stem cell transplant for Acute Myeloid Leukaemia (AML) relative to patients who lacked Bw4 allotypes or who possessed Bw4 allotypes with Thr80 (Marra et al., 2015). Although these genetic associations are broadly consistent with data showing that position 80 impacts recognition of HLA-Bw4 by KIR3DL1, it remains unclear whether Ile80 is predictive of high affinity interactions with KIR3DL1. Similarly, the impact of *KIR3DL1* polymorphism on disease outcome is ill defined. Accordingly, to characterise the spectrum of recognition and the functional consequences of given KIR3DL1 and HLA-Bw4 allotypic pairings, the interactions of a range of HLA-I molecules with representatives of the two inhibitory lineages of KIR3DL1, *005 and *015, together with a common interlineage recombinant, KIR3DL1*001, were compared. Using both KIR3DL1 tetramers and functional assays, Ile80 within the Bw4 motif was observed not to define a high affinity ligand for KIR3DL1. Instead, distinct hierarchies were detected for each KIR3DL1 allotype that assist in reconciling the influence of both KIR3DL1 allotype and HLA-Bw4 polymorphism in determining effective inhibitory capacity. From the ternary crystal structures of KIR3DL1*001, *005 and *015, we show that the dimorphism at position 283 alters the configuration of D1-D2, leading to increased flexibility in KIR3DL1*005, which confers a distinct but broader specificity for HLA-Bw4 allotypes. Our data provide a molecular framework to

interpret the impact of KIR3DL1 polymorphism on HLA-I recognition and can be used to inform disease association studies.

RESULTS

KIR3DL1$^+$ NK cells differentiate between HLA-Bw4 molecules

Although numerous studies have shown that KIR3DL1 interactions with HLA-Bw4 allotypes inhibit NK cell activation, the extent to which this varies between individuals and different HLA-I allotypes has remained unclear (Cella et al., 1994; Gumperz et al., 1997; Gumperz et al., 1995). To address this issue, KIR3DL1$^+$ NK cells obtained from a number of healthy donors were expanded with IL-2 and then incubated either with 721.221 (221) cells which lack endogenous HLA-A, -B and –C, or 221 cells transfected with a range of HLA-I molecules; HLA-B*57:01, -B*58:01 and -A*24:02 that all encode an identical Bw4 motif (NLRIALR), HLA-B*27:05 and HLA-B*44:05 which encode distinct Bw4 motifs containing a Thr at position 80, and HLA-B*08:01, a control allotype that possesses the Bw6 motif (**Figure 1a and b**). The upregulation of CD107a, a marker for degranulation, was assessed by flow cytometry and normalised against the maximal response to the parental 221 cell line (**Figure 1c and d**).

HLA-B*44:05, HLA-B*57:01 and HLA-B*58:01 efficiently inhibited KIR3DL1$^+$ NK cells, while HLA-A*24:02 and HLA-B*27:05 were more limited in this regard, often showing comparable levels of activation to those observed with target cells expressing HLA-B*08:01 (**Figure 1c and d**). These inhibitory effects were not due to CD94-NKGA recognition of HLA-E on the cell surface because all assays were performed in the presence of a CD94 blocking antibody (Pende et al., 2009). In line with this, the pattern of inhibition of was not consistent with CD94-NKG2A/HLA-E dependent mechanism as HLA-B*08:01 and –A*24:02-derived leader sequence peptides (residues 3-11) form more potent CD94-NKG2A ligands when complexed with HLA-E than those derived from other Bw4 allotypes (Borrego et al., 1998)(Brooks et al., 1999)(Petrie et al., 2008). Moreover, variation in the capacity of different HLA-I allotypes to inhibit CD107a expression did not correlate with the level of expression of the transfected HLA-I molecules (**Figure 1e**). Notably, of the cells expressing HLA-Bw4 allotypes, the 221.B5801 transfectants displayed the lowest cell surface expression levels yet had among the most potent inhibitory capacity (**Figure 1d and e**). Similarly, while the expression of HLA-B*27:05 was higher than any other allotype, there was little evidence of Bw4-dependent inhibition of KIR3DL1$^+$ NK cell activation (**Figure 1d**). Possession of Thr80 did not correlate with poor inhibition, as HLA-B*44:05 (Thr80) efficiently inhibited KIR3DL1$^+$ NK cells. Similarly, the presence of Ile80 did not strictly correlate with potent inhibition as while HLA-B*57:01 and -B*58:01 conferred robust inhibition, HLA-A*24:02 was a poor inhibitory ligand

(**Figure 1d**). Additionally, analyses of the capacity of KIR3DL1$^+$ NK cells to degranulate directly *ex vivo* revealed a similar pattern of reactivity. Specifically, HLA-B*57:01 was markedly more inhibitory than allotypes such as HLA-A*24:02 indicating that the variation in inhibitory capacity of different HLA-I allotypes was not simply attributable to the use of *in vitro* activated NK cells (data not shown). Thus, different HLA-Bw4 molecules displayed variable inhibitory capacities between KIR3DL1$^+$ donors that were not closely correlated with the Ile/Thr dimorphism at position 80. Furthermore, the extent to which distinct HLA-I allotypes, in particular HLA-A*24:02 and HLA-B*27:05, inhibited degranulation of KIR3DL1$^+$ NK cells varied markedly between donors and suggested that allotypic differences in KIR3DL1 also influenced ligand recognition.

KIR3DL1 allotypes demonstrate distinct hierarchies of HLA-Bw4 interaction

To account for the impact of KIR3DL1 polymorphism on HLA-Bw4 recognition and to generate a broader perspective on KIR3DL1-HLA-I binding combinations, soluble KIR3DL1*005, *015 and *001 proteins were produced and used to create fluorescently labelled KIR3DL1 tetramers. These KIR3DL1 tetramers were then assessed for their ability to bind an extensive panel of bead-bound HLA-I molecules comprising 100 distinct allotypes. The 25 HLA-I molecules recognised most strongly by KIR3DL1*015 were then ranked and compared against KIR3DL1*001 and KIR3DL1*005. All three KIR3DL1 tetramers displayed a strong preference for HLA-Bw4 molecules (**Figure 2a**). For example, 19 of the top 25 HLA-I allotypes bound by KIR3DL1*015 were HLA-Bw4 molecules (**Figure 2b and c**). Weak binding was observed to the HLA-C molecules HLA-C*07:02, -C*04:01, -C*01:02 and -C*16:01 (up to 12.7% of the maximum signal for KIR3DL1*015 binding to HLA-C*04:01) (**Figure 2b and c)** In contrast, there was negligible binding to HLA-A allotypes, such as HLA-A*02:01, which lacked the Bw4 motif (data not shown). Importantly, the recognition patterns seen in this assay matched well with the data from our degranulation assays where strong recognition of HLA B*57:01 and B*58:01 allomorphs and weaker recognition of HLA-B*27:05 was observed for all three KIR3DL1 allotypes tested (**Figures 2a and c**).

Each of the KIR3DL1 proteins displayed distinct hierarchical preferences for HLA-Bw4 allomorphs, with KIR3DL1*005 being the most divergent. Although KIR3DL1*001 and *015 exhibited a broadly similar preference for HLA-Bw4 allomorphs, differences were apparent (**Figure 2a-c**). For example, KIR3DL1*001 bound more strongly than KIR3DL1*015 to several HLA-Bw4 allomorphs, including HLA-B*44:03 and HLA-B*57:03. Moreover, KIR3DL1*001 bound HLA-B*57:01 and HLA-B*57:03 with similar intensity, whereas KIR3DL1*015 preferentially bound HLA-B*57:01 in comparison to HLA-B*57:03. Thus, there were clear differences between

KIR3DL1*001 and *015 in terms of relative binding strength across different HLA-Bw4 allomorphs and ultimately in the rank order of binding.

While KIR3LD1*005 bound HLA-I allotypes such as HLA-B*57:01 and HLA-B*58:01 with high avidity, there were a number of significant changes in both the rank order of binding and ligand specificity in comparison to both KIR3DL1*001 and KIR3DL1*015 (**Figure 2b and c**). For example, KIR3DL1*001 and *015 bound HLA-A*32:01 very strongly yet there was only a weak interaction with HLA-A*24:02. In contrast, the binding of KIR3DL1*005 to HLA-A*24:02 and HLA-A*32:01 was equivalent, indicating broader recognition of HLA-A allomorphs possessing the Bw4 motif (**Figure 2c**). Additionally, there was substantial variation in KIR3DL1 binding to certain HLA-B allotypes, most notably HLA-B*44:02 and -B*44:03, the former of which was ranked second for KIR3DL1*005 binding, yet interacted relatively poorly with *001 and *015. This overall comparison against KIR3DL1*001 and *015, shows that *005 has both broader and distinct preference for HLA-Bw4 ligands.

This broad screening approach allowed the impact of the Ile/Thr dimorphism at position 80 of HLA-Bw4 allotypes on KIR3DL1 binding to be re-examined (**Figure 2b and c**). When viewed as a group, Ile80^{+} allotypes preferentially interacted with both KIR3DL1*001 and *015 relative to the Thr80^{+} allotypes (**Figure 2a and b**). Nevertheless, the presence of Ile80 did not strictly correlate with strong binding to either KIR3DL1*001 or *015, since HLA-A*24:03 and -B*52:01 (Ile80) interacted more weakly than HLA-B*44:03 and HLA-B*47:01 (Thr80) (**Figure 2a and c**). In contrast, there were no significant differences in the ability of KIR3DL1*005 to discriminate between allotypes that contain Ile80 and Thr80 (**Figure 2b**). These data reveal substantial variation in the specificity between KIR3DL1 allotypes, with KIR3DL1*005 being the most permissive allotype across the range of HLA-Bw4 molecules. Moreover, the Ile80/Thr80 dimorphism of HLA-Bw4 allotypes is not predictive of the strength of ligand recognition by KIR3DL1.

Differences in HLA-Bw4-mediated inhibition between KIR3DL1^{+} NK cell clones

While the interaction of KIR3DL1 tetramers to beads coated with individual HLA-I allotypes generated binding hierarchies for KIR3DL1*005, *015 and *001, it was unclear whether these reflected functional differences. Consequently a panel of NK clones from donors of known KIR3DL1 allotype, LM (*KIR3DL1*001*), RM (*KIR3DL1*002* and **00501*) and BC (*KIR3DL1*00501*), were generated, with the KIR3DL1*002 and *005 populations of donor RM isolated by sorting DX9^{hi} and DX9^{lo} NK cells, respectively (data not shown). KIR3DL1*002 belongs to the **015* lineage, differing from KIR3DL1*015 at only position 238 within the D2

domain (**Figure 3a**). These clones were then assessed for their capacity to lyse either 221 cells or 221 cells transfected with different HLA-I allotypes. Consistent with both their superior capacity to bind KIR3DL1 tetramers (**Figure 2c**) and to inhibit the activation of polyclonal NK cells (**Figure 1d**), the expression of HLA-B*57:01 and HLA-B*58:01 conferred protection from all KIR3DL1^{+} NK cell clones assessed, regardless of KIR3DL1 allotype (**Figure 3b**). This protection was mediated in part through KIR3DL1 as evidenced by the increased lysis following addition of the KIR3DL1/S1 specific antibody, Z27. Similarly, the expression of HLA-B*44:05 also conferred substantial target cell protection irrespective of KIR allotype, again reflecting our observations in assays of bulk NK cell cultures (**Figure 1d, 3b**).

In contrast, NK cell clones expressing either KIR3DL1*001 or KIR3DL1*002 readily lysed 221 cells expressing HLA-A*24:02 whereas the same HLA-I allotype conferred protection from clones expressing KIR3DL1*005 (**Figure 3b**). The extent of this inhibition varied between KIR3DL1*005^{+} donors, with donor BC exhibiting around 40% maximum lysis compared to donor RM at 18%. The pattern of reactivity of NK cell clones towards target cells expressing HLA-B*27:05 was similar to those that expressed HLA-A*24:02, in that while HLA-B*27:05 did not confer significant protection from clones expressing KIR3DL1*002, it nevertheless conferred significant protection from lysis by clones from donor RM that expressed the *005 allotype. This broadly reflected what was observed in the KIR3DL1 tetramer binding assay since KIR3DL1*005 bound to both HLA-A*24:02 and HLA-B*27:05-coated beads more strongly than the other KIR3DL1 allotypes, albeit with weaker avidity than was observed for HLA-B*57:01, -B*58:01 and B*44:02. Nevertheless, the binding of KIR3DL1*005 to HLA-B*27:05 was still stronger than that to any non-Bw4 allotype. Taken together the functional and bead binding data suggest that while HLA-B*27:05 may interact with KIR3DL1*005 with low avidity, it is still able to function as a ligand. In contrast, KIR3DL1*001 and **015*-lineage molecules appear to have a higher binding threshold for functional ligand recognition.

To confirm and extend these analyses, an additional panel of clones was established from another four donors. The KIR3DL1 allele expressed in each clone was determined by sequencing KIR3DL1 cDNAs amplified from RNA, identifying clones expressing the lineage defining KIR3DL1*005 and *015, as well as KIR3DL1*002 and *009. Uniquely, KIR3DL1*009 possesses the D0 domain of KIR3DS1 coupled with the *001 D1-D2 domains (**Figure 3a**) and has been suggested to display weaker binding to HLA-Bw4 than that KIR3DL1*001 or *005 (Mulrooney et al., 2015). These NK cell clones were then cocultured with either parental or HLA-I transfected 221 cells and the expression of CD107a assessed by flow cytometry. The expression of CD107a by KIR3DL1*001^{+},

*002$^+$ and *005$^+$ NK clones was consistent with the data obtained from the cytotoxicity assays (**Figure 3c**). Namely, HLA-B*57:01, HLA-B*58:01 and HLA-B*44:05 effectively inhibited degranulation by all KIR3DL1 allotypes tested, whereas HLA-A*24:02 only inhibited activation of the KIR3DL1*005$^+$ clone. Both KIR3DL1*01502 and *009 resembled KIR3DL1*001 in their recognition of HLA-B*57:01, HLA-B*58:01 and HLA-B*44:05 where all three HLA-I allotypes inhibited CD107a expression. In contrast, the expression of HLA-A*24:02 had only a modest inhibitory impact on degranulation of NK cell clones expressing KIR3DL1*001, *002, *015:02 and *009 whereas HLA-A*24:02 inhibited activation of the clone expressing KIR3DL1*005. Taken together, the data derived from the analyses of 35 NK clones derived from 7 donors expressing a range of KIR3DL1 allotypes have identified clear specificity differences between KIR3DL1*005 and a number of KIR3DL1 allotypes that share common polymorphisms across the D1 and D2 domains, notably residues 182 and 283. The data highlight that the Bw4 recognition preferences of KIR3DL1 do not simply segregate with the presence of an Ile or Thr at position 80. Moreover the data suggest that KIR3DL1*005 has an expanded ligand range relative to allotypes of the KIR3DL1*015 lineage or the recombinant allotypes KIR3DL*001 and *009. Accordingly, there is a functional hierarchy of HLA-Bw4 recognition that is dependent on KIR3DL1 polymorphism.

Molecular basis of KIR3DL1 polymorphism on HLA class I recognition

To provide molecular insights into the altered patterns of ligand recognition by KIR3DL1*001, *005 and *015, the structures of KIR3DL1*005 and *015 in complex with HLA-B*57:01 were determined to 2.3 and 2.5 Å, respectively (**Table 1**). The KIR3DL1 complexes were crystallised in the same conditions and in the same space group (**Table 1**). The high quality of the resultant structures allowed for direct comparison with the previously determined KIR3DL1*001-peptide-HLA-B*57:01 complex (Vivian et al., 2011). The overall binding mode of these three KIR3DL1-peptide-HLA-I ternary complexes was similar. Specifically, the D0 domain clamped around the side of HLA-B*57:01, abutting β2-microglobulin, while the D1 and D2 domains were positioned above the C-terminal end of the peptide-binding cleft, with the D1 domain interacting with the Bw4 motif (**Figure 4a and b**). The KIR3DL1*005 and *015 complexes maintained key contacts with HLA-B*57:01 that were identified from structural and mutagenesis studies of KIR3DL1*001 recognition (Vivian et al., 2011). In particular, the interactions between positions Phe9 on the D0 domain and residues 17-19 on HLA-B*57:01, and the interactions between Tyr200, Phe276 and Glu282 on the D2 domain and residue Lys146 on the α2 helix of HLA-B*57:01 were conserved (**Figure 4b**). Similarly, the contacts between the KIR3DL1 residue Leu166 and Ile80 in the Bw4 motif and Ser8 in the bound peptide were preserved across all KIR3DL1 ternary complexes (**Figure 4b**). The total buried surface area at the complex interfaces was also comparable, (KIR3DL1*001 =

1790 Å^2, *005 = 1870 Å^2 and *015 = 2060 Å^2). Accordingly, the three KIR3DL1 allomorphs use a similar inventory of principal residues to recognise HLA-B*57:01 complexed with the LF9 peptide.

Despite this consensus docking mode, differences were observed between the three ternary complexes attributable to polymorphic residues that distinguish KIR3DL1*001, *005 and *015. KIR3DL1*005 and *015 differ at seven amino acids, five in the signal sequence-D0 domain and two in the D1-D2 domains. Across the extracellular regions examined, KIR3DL1*015 differs from *005 at positions Val47Ile, Leu54Ile, Pro182Ser and Trp283Leu. As KIR3DL1*001 is a recombinant of the D0 from *005 and the D1-D2 from *015 it thus differs from *015 at positions 47 and 54 and from *005 at positions 182 and 283 (**Figure 4a**).

The docking of the D0 and D1 domains to HLA-B*57:01-LF9 was distinct between the complexes, despite a common 80° hinge angle about the D0-D1 domains (**Figure 4c and d**). Notably, the KIR3DL1*005 D0-D1 domain arrangement was identical to that observed in *015, both of which were distinct from that of *001. More specifically, compared to the KIR3DL1*001 complex, the *005 and *015 complexes displayed a 3° difference in the crossing angle of the D1 domain and a 1 Å translational shift of the D0 domain. These two D0-D1 profiles were coincident with two distinct conformations of the C-C′ loop (**Figure 5a**)**.** Such conformations are also observed in complexes of KIR3DL1*001 with HLA-B*57:01 bound to different peptides (*unpublished data, JPV*). Thus, the C-C′ loop conformation varies as a function of both the bound peptide and the KIR3DL1 allotype.

The hinge angle between the D1 and D2 domains clearly distinguished the KIR3DL1*001 and *015 complexes from that of *005. This angle in KIR3DL1*001 and *015 was more acute (76°) than that observed in *005 (80°) (**Figures 4c and d**). Centrally placed to influence the inter-domain hinge angle was the dimorphic residue 283, residing on the F' strand of the D2 domain, interconnecting the D1 and D2 domains. Trp283 in KIR3DL1*001 and *015 and Leu283 in *005 were positioned in a hydrophobic pocket and made similar contacts to neighbouring residues including contacts to Leu112 and Val195 on the D1 domain and His233, Phe273 and Ser275 on the D2 domain (**Figure 5b and c**). Unique to Trp283 was a H-bond from the indole nitrogen to Pro280 that aided the alignment of Trp283. These contacts were of importance to the hinge angle, with Trp283 oriented parallel to the axis of the D1-D2 hinge. The Trp283 therefore had a narrower profile than the Leu283 allowing for a tighter hinge angle (**Figures 4c, 5b and c**).

The differences in the relative angles of the KIR3DL1 domains had a modest impact on contacts with HLA-B*57:01-LF9. Indeed, all contacts were preserved to residues known to be critical for the

interaction with KIR3DL1*001 (Vivian et al., 2011). However, differences were observed at the short helix between the E-F strands, as Met165 on KIR3DL1*005/*015 formed an additional peptide contact to Thr6. Further, the 8° difference in the crossing-angle of the D2 domain (**Figure 4c and d**) enabled additional contacts between the F-strand residue His278 on KIR3DL1*001/*015 and Ile142 and Tyr84 of the HLA molecule (**Figure 5d**). Combined with the wider hinge angle for the D1-D2 domains of KIR3LD1*005, this translates to a different docking mode for the *005 allotype, which further associates with an impact on HLA-Bw4 recognition.

Increased mobility of ligand binding loops within KIR3DL1*005.

We hypothesised that the wider D1-D2 angle in KIR3DL1*005 relative to either *001 or *015 would confer a greater degree of flexibility around the peptide-HLA-I binding site, thereby allowing KIR3DL1*005 to tolerate a broader range of ligands. To test this hypothesis, solution phase deuterium exchange experiments were performed on KIR3DL1*001, *015 and *005. In these experiments increased levels of hydrogen exchange with deuterium are associated with a greater degree of mobility. Strikingly, mass spectrometric analysis showed that the greatest difference in the extent of deuterium exchange was located within ligand binding loops of KIR3DL1 (**Figures 6a-c**). These loops were the D1 C-C′ loop (residues 133-145) (**Figure 6a**), the D1 E-F loop (residues 160-173) (**Figure 6b**) and D1/D2 hinge loop (residues 194-205) (**Figure 6c**). Moreover, in each case, there was significantly more deuterium exchange in KIRDL1*005 relative to *001 or *015 (**Figures 6a-c**). The extent of exchange in the latter two allotypes was similar. Deuterium exchange data was also collected on peptide fragments from the D2 C-C′-D strands and the D-E loop (residues 233-253) (**Figure 6d**), the D2 E-F loop and F-strand (residues 260-274) (**Figure 6e**) and the D2 F-F′ and F′-G loops (residues 275-292) (**Figure 6f**). For each of these D2 peptide fragments there was no difference in the extent of deuterium exchange. Collectively, these data show that the ligand binding loops of the D1 and the D1/D2 hinge-loop of KIR3DL1*005 are more dynamic than either *001 or *015, suggesting that the wider hinge angle ultimately allows the *005 allotype to adopt conformations that can accommodate microvariation in ligand structure resulting from both HLA-I polymorphism and variability in the associated peptide repertoire.

DISCUSSION

High avidity interactions between inhibitory KIRs and their HLA-I ligands are thought to result in well-educated NK cells with potent effector functions that are highly responsive to cells with reduced surface expression of HLA-I. Such interactions have been proposed to be associated with poor outcomes in malignancies such as AML, where there is little evidence of HLA-I downregulation, and with improved viral control in HIV-infected individuals (Cooley et al., 2014)

(Marra et al., 2015). However, the molecular signatures that define "high affinity" interactions are themselves, poorly defined. Specifically with respect to KIR3DL1, the presence of an Ile80 within the Bw4 motif has been thought to act as a signature for potent ligands, particularly for KIR3DL1 allotypes with high levels of cell surface expression which ultimately translated into clinical associations with disease progression in the setting of HIV (Martin et al., 2007) (Cella et al., 2000) (Yawata et al., 2006a). A number of studies following a similar approach have found associations between the presence of KIR3DL1 and $Bw4^{80I}$ allotypes with the probability of relapse in patients receiving HSCT for AML or the simply with presence of $Bw4^{80I}$ in diseases such as Behcet's disease and hepatitis B-associated hepatocellular carcinoma, often in association with *KIR3DS1* (Kuranov et al., 2014) (Marra et al., 2015) (Pan et al., 2011). Although residue 80 clearly plays a central role in KIR3DL1 recognition, the functional and binding data presented here demonstrate that the presence of Ile80 alone is insufficient for strong engagement of KIR3DL1. Notably, there were marked differences between different $Ile80^{+}$ Bw4 allotypes in terms of their capacity to inhibit target cell lysis by clonal or polyclonal $KIR3DL1^{+}$ NK cells. For example, while HLA-B*57:01 and HLA-B*58:01 readily conferred protection from lysis by $KIR3DL1^{+}$ NK cells, HLA-A*24:02 exhibited considerably weaker effects, despite the fact that all three HLA-I allotypes shared an identical sequence spanning the Bw4 motif. Extending these functional observations, our broad screening of HLA-I binding preferences using KIR3DL1 tetramers showed that while Bw4 molecules possessing Ile80 were among the best ligands regardless of KIR3DL1 allotype, several $Ile80^{+}$ allotypes such as HLA-A*23:01, HLA-A*24:02 and HLA-B*52:01 were poorly recognised. Indeed, these allotypes were weaker ligands than HLA-B*44:02, HLA-B*44:03 and HLA-B*47:01, all of which encode Thr80. Thus, while many potent ligands possess Ile80, the Ile/Thr dimorphism at residue 80 cannot strictly be used as a marker of KIR3DL1 ligand affinity. This has important implications for disease association studies based around the presence or absence of Bw4 allotypes that have Ile80. The majority of $Bw4^{80I}$ alleles that act as high avidity ligands for KIR3DL1 are themselves relatively common, at least in certain ethnicities. For example the overall frequency of HLA-B*57:01 is typically reported to vary between 1-3% in most studies but may be significantly higher in those of Indian decent, while the overall frequency of HLA-B*58:01 is ~3%, can be very common in African populations (Solberg et al., 2008) (Cao et al., 2001). However we have shown that other $Bw4^{80I}$ alleles such as HLA-A*24:02 and –B*52:01, both of which can be very common (>5%) in certain Asian populations, can be relatively poor ligands, at least for certain KIR3DL1 allotypes(Cao et al., 2001; Solberg et al., 2008). The inclusion of the latter alleles into groups of alleles that are considered to be high avidity/function may mean the strength of the associations reported with diseases in HIV and AML are underestimated. Similarly the exclusion of common $Bw4^{80T}$ allotypes such as HLA-B*44:03 that interact robustly with KIR3DL1*015, *001 and *005

may also serve to diminish the statistical strength of these disease associations. As such, the data here provide an empirical rationale for the re-evaluation of disease association studies that are genuinely based on the avidity of the KIR3DL1/ligand.

Further compounding the difficulty of interpreting associations of KIR3DL1 and Bw4 alleles with clinical outcomes is allelic variation in *KIR3DL1* itself. Our data, based on the binding of KIR3DL1 allotypes representative of the two major inhibitory allelic lineages (*015 and *005) along with an interlineage recombinant (*001) has systematically evaluated the extent to which allotypic variation in KIR3DL1 modulates receptor specificity. Notably KIR3DL1*015 bound to its ligands with lower avidity than either *001 or *005. Moreover, the polymorphic differences between KIR3DL1*001 and *015 did not simply impact the overall level of binding but rather resulted in subtle differences in the specificity between KIR3DL1*015 and *001. More striking still were the differences in binding profile between KIR3DL1*005 and both KIR3DL1*001 and *015. Not only did KIR3DL1*005 bind a greater range of HLA-I allotypes but there were also marked differences in the hierarchy of HLA-I allotype binding. When assessed in functional assays using NK cell clones, the altered binding hierarchy between different KIR3DL1 allotypes was manifest in an altered specificity. Namely a larger spectrum of HLA-I allotypes were able to inhibit activation of NK cell clones expressing KIR3DL1*005 compared with other allotypes examined including KIR3DL1*001, *015, *009 and *002.

Previous findings had suggested that the Trp/Leu dimorphism at residue 283 of KIR3DL1 was critical in defining the *015 and *005 lineages of KIR3DL1 and shown that the introduction of Leu283 in KIR3DL1*001, *007 and *015 enhanced binding to Bw4 tetramers possessing Thr80 (O'Connor et al., 2014; Sharma et al., 2009). Here we show that KIR3DL1 allotypes possessing Trp283 had a more restricted range of ligands as assessed by both binding and functional studies, than KIR3DL1*005 which possesses a Leu at this position. The differences between KIR3DL1*015, *001 and 005 centre on a limited set of dimorphic residues; residues 2, 47 and 54 on the D0 domain (distal to the HLA binding interface), residue 182 on the D1 domain (at the D0-D1 domain interface) and residue 283 (at the D1-D2 domain interface). Sharma *et al* have shown that KIR3DL1*001 bound more strongly to HLA-A*24:02 tetramers complexed with a nef-encoded peptide than either KIR3DL1*005 or KIR3DL1*015 suggesting some degree of synergy between the D0 and D1-D2 domains in the recombinant allele (Sharma et al., 2009). However given that ligand recognition by KIR3DL1 is acutely dependent on the sequence of the HLA-associated peptide, it is unclear whether this synergism was a general feature of ligand recognition by these allotypes (Malnati et al., 1995; Thananchai et al., 2007). Regardless, that polymorphisms distal to

the HLA binding interface are able to impact ligand binding avidity implies an indirect molecular mechanism. A number of studies have noted such effects, particularly from allotypes bearing polymorphisms at residues 58, 92 and 238 (Carr et al., 2005; Mulrooney et al., 2015; Thananchai et al., 2007). Interestingly, our data analysing the structures of KIR3DL1*001, *005 and *015 identified two conformations of the D0-D1 domains. However, these differing docking conformations were not wholly attributable to KIR3DL1 polymorphisms as different docking angles have been observed between KIR3DL1*001 and HLA-B*57:01 in complex with different peptides (*unpublished data, JPV*). This indicates that there is a degree of flexibility across the three KIR3DL1 domains whose ultimate arrangement, though in part regulated by polymorphic residues that are spatially remote from the ligand-binding site, are also subject to the nature of the HLA allotype and the associated peptide.

The structural data show that the Leu-Trp dimorphism at position 283 is associated with an altered juxtapositioning of the D1 and D2 domains, resulting in a subtle realignment of the residues contacting the HLA-B*57:01-LF9 complex. Moreover, the deuterium exchange data revealed that the larger hinge angle associated with the presence of Leu283 confers a degree of flexibility, particularly over the KIR3DL1 loops, which are intimately involved in recognition of both the peptide and the Bw4 motif. These findings suggest that the increased flexibility of the ligand-binding region allows KIR3DL1*005 to better accommodate variability in the sequence of peptides bound to Bw4 allotypes. Consistent with this notion, the introduction of Leu283 into both KIR3DL1*001 and *015 substantially enhanced binding to HLA-B*57:01 complexed with an escape variant of the HIV-encoded peptide TW10 (O'Connor et al., 2014).

Predicting the functional outcomes that result from KIR3DL1–HLA-I interactions is complex and is likely based on the conjoined effects of avidity, surface expression of both receptor and ligand, as well as cell-surface clustering and the signalling potential of the receptor(Carr et al., 2005) (Mulrooney et al., 2015; Pando et al., 2003). Although it is clear that a number of polymorphisms in KIR3DL1 can impact functional responses to cells bearing HLA-Bw4 molecules, our study has elucidated the effect of polymorphisms within the two major KIR3DL1 lineages that combine to influence binding avidity and ultimately specificity. Accordingly, we have demonstrated distinct recognition hierarchies and identified a broad conceptual framework to understand the impact of polymorphism across the KIR3DL1-HLA-I axis that will result in an improved understanding of KIR3DL1/HLA pairings in disease and transplant settings.

MATERIALS AND METHODS

Cell lines

The human HLA class Ia-deficient B-lymphoblastoid cell line 721.221 (221) was transfected with HLA-A*24:02, HLA-B*08:01, HLA-B*27:05, HLA-B*44:05 or HLA-B*57:01 via electroporation at 200V and 975μF (Saunders et al., 2015). 221.B58 cells were a generous gift from Peter Parham (Stanford University, CA). All cells were maintained in RPMI 1640 medium (Lonza, Basel, Switzerland) supplemented with antibiotics and 10% fetal bovine serum (FBS; Lonza).

Purification of NK cells and generation of KIR3DL1$^+$ NK cell clones

Human PBMCs were isolated from healthy blood donors by Ficoll/Hypaque density gradient centrifugation. Negative selection of untouched NK cells was performed using RosetteSep™ or EasySep™ Human NK Cell Enrichment Kits according to the manufacturer's instructions (Stemcell Technologies Vancouver, Canada). NKG2A$^-$KIR3DL1$^+$ (Z199$^-$DX9$^+$) cells were isolated by flow cytometry at >95% purity using a FACSAria II (BD Biosciences, Franklin Lakes, NJ). KIR3DL1$^+$ NK cells were cultured on irradiated feeder cells in the presence of 100 U/mL rhIL2 (Proleukin; Chiron Corp., Emeryville, CA) and 1.5 ng/mL PHA (Gibco Ltd., Paisley, Scotland) and cloned by limiting dilution. Proliferating NK cell clones were analysed for KIR3DL1 expression and the absence of NKG2A (Z270) before use in functional experiments. NK cells were maintained in RPMI 1640 supplemented with antibiotics, 10% FBS and 100 U/mL IL-2. For donors with an unknown *KIR3DL1* allele, the expressed KIR3DL1 molecule was sequenced from extracted RNA (Saunders et al., 2015). All studies were done in accordance with approvals from the Human Research Ethics Committee, University of Melbourne or the Liguria Regional Committee.

NK cell cytotoxicity

NK cell-mediated cytotoxicity was assessed in standard 4 hour chromium-release assays (Pende et al., 2009). Briefly, effector cells were incubated with ^{51}Cr-labeled 221 transfectants at various effector:target (E:T) ratios. For masking experiments, KIR3DL1$^+$ NK cell clones were incubated with ^{51}Cr-labeled target cells, either in culture medium alone or in the presence of an anti-KIR3DL1/S1 mAb (clone Z27, IgG1) at a concentration of 10 μg/mL. Data were normalised to the maximal lysis of parental 221 target cells detected in the absence of Z27 blocking.

CD107a assay

NK cells and 221 transfectants were mixed at a 1:1 ratio and incubated for 1 hour in the presence of anti-CD107a-PE (BD Biosciences) before the addition of monensin. The blocking antibody Y9 was added to NKG2A$^+$ NK cells prior to mixing with targets. After a further 3 hour incubation, cells

were stained with anti-NKB1-FITC (anti-KIR3DL1; BD Biosciences) and anti-CD56-APC (BD Biosciences), fixed in 2% paraformaldehyde and analysed by flow cytometry. The percentage of KIR3DL1^{+} NK cells expressing CD107a was determined using FlowJo software (TreeStar Inc., Ashland, OR) and normalised to maximal CD107a expression in the presence of parental 221 target cells.

Cloning and expression of KIR3DL1

The extracellular domains of KIR3DL1*001/*005/*015 (residues 1–299) were subcloned into vectors for insect cell and mammalian cell expression. For insect cell expression, the genes were subcloned into a modified baculoviral pFastBac-expression vector (Invitrogen, Carlsbad, CA) containing a secretion signal peptide sequence, an N-terminal hexa-histidine tag and a C-terminal BirA-tag (Stifter et al., 2014). For mammalian expression, the genes were subcloned into the pHLSec-expression vector containing a secretion signal peptide sequence and an N-terminal hexa-histidine tag (Aricescu et al., 2006). Insect cell expression of KIR3DL1 was performed by baculoviral infection of BTI-TN-5B1-4 cells (Hi-5 cells; Invitrogen). Mammalian expression was performed by transient transfection of HEK293S GnTI^{-} cells (Aricescu et al., 2006). From both cell lines, KIR3DL1 was secreted into the expression media and purified by binding to nickel sepharose resin followed by size exclusion chromatography (S200 16/60 column; GE Healthcare, Little Chalfont, UK). The insect cell material was used for single-antigen bead experiments but was not amenable to crystallization. The mammalian cell material was used in X-ray crystallography studies following overnight incubation with endoglycosidase H (New England Biolabs, Ipswich, MA).

Bead assay

HLA-I recognition by KIR3DL1 allotypes was assessed through binding of KIR3DL1 tetramers to beads coated with a panel of 100 different HLA-A, -B and -C molecules (LABScreen HLA Class I Single Antigen; One Lambda, Canoga Park, CA). Phycoerythrin-conjugated KIR3DL1 tetramer (5 μg per test) was incubated with beads for 30 minutes at room temperature in the dark in phosphate-buffered 300mM NaCl (PBS-300) with 5% foetal calf serum (AusGeneX, Molendinar, Australia). The beads were then washed three times in PBS-300 with 0.05% Tween 20 and resuspended in PBS-300. Binding was measured on a luminex platform (LABScan™ 100; One Lambda) through identification of the individual HLA allotypes via unique bead labeling and detection of tetramer fluorescence intensity on each bead set. Normalised fluorescence values for analysis were obtained using the HLA Fusion software suite (One Lambda) that subtracted background values using the following formula:

$$(\boldsymbol{S\#N - SNC\ bead}) - (\boldsymbol{BG\#N - BGNC\ bead})$$

(**S#N** = Sample-specific fluorescence value (trimmed mean) for bead #N; **SNC bead** = Sample-specific fluorescence value for Negative Control (nude) bead; **BG#N** = Background Negative Control fluorescence value for bead #N; **BGNC bead** = Background Negative Control fluorescence value for Negative Control bead). Negative control samples were obtained using unconjugated streptavidin-PE in place of the conjugated KIR tetramer. To obtain binding values for each HLA class I, mean fluorescence intensity (MFI) values for an isotype control (a PE-conjugated IgG) were subtracted from the raw values obtained for each experiment and recognition was assessed as being higher than that of the tetramer to beads without conjugated HLA class I. MFI values were normalised to the highest value for each experiment and then averaged over three experiments.

Expression and purification of HLA-B*57:01

Plasmids encoding HLA-B*57:01 and β2-microglobulin were expressed separately in *E. coli* and refolded in the presence of the peptide LSSPVTKSF (LF9). Purification of the HLA-B*57:01-LF9 complex was carried out as described previously (Chessman et al., 2008).

Crystallization, data collection, structure determination and refinement

KIR3DL1*005 and *015 expressed in mammalian HEK 293S GnTI$^-$ cells were concentrated to 12 mg/mL and combined with HLA-B*57:01-LF9 at a 1:1 molar ratio. The KIR3DL1-peptide-HLA-B*57:01 complexes were crystallized at 294K by the hanging-drop vapour-diffusion method from a solution comprising 14–18% PEG 3350, 2% tacsimate pH 5.0 and 0.1 M tri-sodium citrate pH 5.6. Prior to data collection, the crystals were equilibrated in crystallization solution with 35% PEG 3350 added as a cryoprotectant and then flash-cooled in a stream of liquid nitrogen at 100K. X-ray diffraction data were collected at the MX2 beamline (Australian Synchrotron, Victoria). The data were recorded on a Quantum-315 CCD detector and were integrated and scaled using MOSFLM and SCALA from the CCP4 program suite (Collaborative Computational Project, 1994; Evans, 2006). Details of the data processing statistics are summarised in **Table 1**. The crystal structures were determined by molecular replacement, as implemented in PHASER (McCoy et al., 2007), with KIR3DL1*001-LF9-HLA-B*57:01 used as the search model (Protein Data Bank accession number: 3VH8 (Vivian et al., 2011)). Refinement of the models proceeded with iterative rounds of manual building in COOT (Emsley and Cowtan, 2004) and refinement in PHENIX (Adams et al., 2010). The final models comprised N-acetylglucosamine groups at Asn71, Asn158 and Asn252. The structures were validated with MOLPROBITY (Chen et al., 2010). Refinement statistics are

summarised in **Table 1**. Coordinates and structure factors were deposited in the Protein Data Bank (KIR3DL1*005-HLA-B57:01-LF9, 5B38; KIR3DL1*015-HLA-B57:01-LF9, 5B39).

Peptide mapping by HPLC-tandem mass spectrometry

Peptide mapping was performed as described previously (Tsutsui et al., 2006). Briefly, 5 μg of purified KIR3DL1 (in 100 μL of 100 mM Tris pH 7.4 and 80 mM NaCl) was mixed with 95 μL of 0.5% trifluoroacetic acid (TFA; pH 2.4). Porcine pepsin (5 μg) dissolved in 0.05% (v/v) TFA was then added over five minutes on ice. The digested sample was injected into a micropeptide trap (Grace, Columbia, MD) connected to a Everest C18 column (50 mm x 1 mm, 5 μm; Grace) and a micrOTOF mass spectrometer (Bruker, Billerica, MA). Peptidic fragments were eluted with a gradient of acetonitrile at a flow rate of 50 μL/min for tandem mass spectrometry to sequence each peptidic fragment. Peptidic fragments were identified using the Mascot search algorithm.

Hydrogen deuterium exchange analyses

Soluble KIR3DL1 (in 100 mM Tris pH 7.4 and 50 mM NaCl) was diluted 24-fold in 100 mM Tris pH 7.4 and 80 mM NaCl dissolved in D_2O (Cambridge Isotope Laboratories, Tewksbury, MA) at 25°C. The reaction was quenched at different time points by adding an equal volume of 0.5% TFA (pH 2.4) followed by rapid freezing. The first experimental time point was measured 10 seconds after initiation of the experiment. Frozen samples were thawed and digested with 5 μg of pepsin on ice for five minutes, then injected immediately into a micropeptide trap connected to a C18 column (Grace) and a micrOTOF mass spectrometer (Bruker). Peptides were eluted in 12 minutes using a gradient of 10−45% acetonitrile at a flow rate of 50 μL/min. The micropeptide trap and C18 column were immersed in ice to minimize back exchange. To correct for any back exchange of hydrogen atoms during pepsin digestion and HPLC-MS, a fully deuterated sample was prepared by incubating 5 μg of KIR3DL1 in 6 M guanidine deuterochloride, 50 mM Tris pH 8 and 50 mM NaCl for 60 minutes at 25°C. The deuterium incorporation of each peptidic fragment, corrected for the back exchange, was calculated using the following equation: $D/N=[(m-m_{0\%})/(m_{100\%}-m)]$, where m is the mass of deuterated peptidic fragment, $m_{0\%}$ and $m_{100\%}$ are the mass of the unlabeled and fully deuterated peptidic fragments, respectively, N is the total number of exchangeable amide hydrogen atoms in each peptidic fragment, and D is the number of amide hydrogen atoms incorporated in each peptide.

ACKNOWLEDGEMENTS

This work was funded by grants from the National Health and Medical Research Council (JR, AGB, DWM and JPV) and the worldwide cancer research organisation. This work was funded in

part by the intramural program of the National Cancer Institute. DAP is supported by a Wellcome Trust Senior Investigator Award. JR is supported by an Australia Fellowship from the NHRMC. JPV is supported by an Australian Research Council DECRA Fellowship. This research was undertaken in part on the MX2 beamline at the Australian Synchrotron, Victoria, Australia. The authors declare no competing financial interests.

REFERENCES

Adams, P.D., P.V. Afonine, G. Bunkoczi, V.B. Chen, I.W. Davis, N. Echols, J.J. Headd, L.W. Hung, G.J. Kapral, R.W. Grosse-Kunstleve, A.J. McCoy, N.W. Moriarty, R. Oeffner, R.J. Read, D.C. Richardson, J.S. Richardson, T.C. Terwilliger, and P.H. Zwart. 2010. PHENIX: a comprehensive Python-based system for macromolecular structure solution. *Acta Crystallogr D Biol Crystallogr* 66:213-221.

Aricescu, A.R., W. Lu, and E.Y. Jones. 2006. A time- and cost-efficient system for high-level protein production in mammalian cells. *Acta crystallographica. Section D, Biological crystallography* 62:1243-1250.

Borrego, F., M. Ulbrecht, E.H. Weiss, J.E. Coligan, and A.G. Brooks. 1998. Recognition of human histocompatibility leukocyte antigen (HLA)-E complexed with HLA class I signal sequence-derived peptides by CD94/NKG2 confers protection from natural killer cell-mediated lysis. *J Exp Med* 187:813-818.

Brooks, A.G., F. Borrego, P.E. Posch, A. Patamawenu, C.J. Scorzelli, M. Ulbrecht, E.H. Weiss, and J.E. Coligan. 1999. Specific recognition of HLA-E, but not classical, HLA class I molecules by soluble CD94/NKG2A and NK cells. *J Immunol* 162:305-313.

Cao, K., J. Hollenbach, X. Shi, W. Shi, M. Chopek, and M.A. Fernández-Viña. 2001. Analysis of the frequencies of HLA-A, B, and C alleles and haplotypes in the five major ethnic groups of the United States reveals high levels of diversity in these loci and contrasting distribution patterns in these populations. *Human Immunology* 62:1009-1030.

Carr, W.H., M.J. Pando, and P. Parham. 2005. KIR3DL1 polymorphisms that affect NK cell inhibition by HLA-Bw4 ligand. *J Immunol* 175:5222-5229.

Cella, M., A. Longo, G.B. Ferrara, J.L. Strominger, and M. Colonna. 1994. NK3-specific natural killer cells are selectively inhibited by Bw4-positive HLA alleles with isoleucine 80. *J Exp Med* 180:1235-1242.

Cella, M., H. Nakajima, F. Facchetti, T. Hoffmann, and M. Colonna. 2000. ILT receptors at the interface between lymphoid and myeloid cells. *Curr Top Microbiol Immunol* 251:161-166.

Chen, V.B., W.B. Arendall, 3rd, J.J. Headd, D.A. Keedy, R.M. Immormino, G.J. Kapral, L.W. Murray, J.S. Richardson, and D.C. Richardson. 2010. MolProbity: all-atom structure validation for macromolecular crystallography. *Acta Crystallogr D Biol Crystallogr* 66:12-21.

Chessman, D., L. Kostenko, T. Lethborg, A.W. Purcell, N.A. Williamson, Z. Chen, L. Kjer-Nielsen, N.A. Mifsud, B.D. Tait, R. Holdsworth, C.A. Almeida, D. Nolan, W.A. Macdonald, J.K. Archbold, A.D. Kellerher, D. Marriott, S. Mallal, M. Bharadwaj, J. Rossjohn, and J. McCluskey. 2008. Human leukocyte antigen class I-restricted activation of CD8+ T cells provides the immunogenetic basis of a systemic drug hypersensitivity. *Immunity* 28:822-832.

Collaborative Computational Project, N. 1994. The CCP4 suite: programs for protein crystallography. *Acta crystallographica. Section D, Biological crystallography* 50:760-763.

Cooley, S., D.J. Weisdorf, L.A. Guethlein, J.P. Klein, T. Wang, S.G. Marsh, S. Spellman, M.D. Haagenson, K. Saeturn, M. Ladner, E. Trachtenberg, P. Parham, and J.S. Miller. 2014.

Donor killer cell Ig-like receptor B haplotypes, recipient HLA-C1, and HLA-C mismatch enhance the clinical benefit of unrelated transplantation for acute myelogenous leukemia. *J Immunol* 192:4592-4600.

Emsley, P., and K. Cowtan. 2004. Coot: model-building tools for molecular graphics. *Acta Crystallogr D Biol Crystallogr* 60:2126-2132.

Evans, P. 2006. Scaling and assessment of data quality. *Acta Crystallogr D Biol Crystallogr* 62:72-82.

Gardiner, C.M., L.A. Guethlein, H.G. Shilling, M. Pando, W.H. Carr, R. Rajalingam, C. Vilches, and P. Parham. 2001. Different NK cell surface phenotypes defined by the DX9 antibody are due to KIR3DL1 gene polymorphism. *J Immunol* 166:2992-3001.

Gumperz, J.E., L.D. Barber, N.M. Valiante, L. Percival, J.H. Phillips, L.L. Lanier, and P. Parham. 1997. Conserved and variable residues within the Bw4 motif of HLA-B make separable contributions to recognition by the NKB1 killer cell-inhibitory receptor. *J Immunol* 158:5237-5241.

Gumperz, J.E., V. Litwin, J.H. Phillips, L.L. Lanier, and P. Parham. 1995. The Bw4 public epitope of HLA-B molecules confers reactivity with natural killer cell clones that express NKB1, a putative HLA receptor. *J Exp Med* 181:1133-1144.

Kuranov, A.B., I. Kötter, J.C. Henes, S.T. Abisheva, I. Steiert, F. Riewerts, K.T. Momynaliev, and C.A. Müller. 2014. Behçet's disease in HLA-B*51 negative Germans and Turks shows association with HLA-Bw4-80I. *Arthritis Research & Therapy* 16:1-6.

Litwin, V., J. Gumperz, P. Parham, J.H. Phillips, and L.L. Lanier. 1994. NKB1: a natural killer cell receptor involved in the recognition of polymorphic HLA-B molecules. *J Exp Med* 180:537-543.

Ljunggren, H.G., and K. Karre. 1990. In search of the 'missing self': MHC molecules and NK cell recognition. *Immunol Today* 11:237-244.

Luque, I., R. Solana, M.D. Galiani, R. Gonzalez, F. Garcia, J.A. Lopez de Castro, and J. Pena. 1996. Threonine 80 on HLA-B27 confers protection against lysis by a group of natural killer clones. *European journal of immunology* 26:1974-1977.

Malnati, M.S., M. Peruzzi, K.C. Parker, W.E. Biddison, E. Ciccone, A. Moretta, and E.O. Long. 1995. Peptide specificity in the recognition of MHC class I by natural killer cell clones. *Science* 267:1016-1018.

Marra, J., J. Greene, J. Hwang, J. Du, L. Damon, T. Martin, and J.M. Venstrom. 2015. KIR and HLA Genotypes Predictive of Low-Affinity Interactions Are Associated with Lower Relapse in Autologous Hematopoietic Cell Transplantation for Acute Myeloid Leukemia. *The Journal of Immunology* 194:4222-4230.

Martin, M.P., Y. Qi, X. Gao, E. Yamada, J.N. Martin, F. Pereyra, S. Colombo, E.E. Brown, W.L. Shupert, J. Phair, J.J. Goedert, S. Buchbinder, G.D. Kirk, A. Telenti, M. Connors, S.J. O'Brien, B.D. Walker, P. Parham, S.G. Deeks, D.W. McVicar, and M. Carrington. 2007. Innate partnership of HLA-B and KIR3DL1 subtypes against HIV-1. *Nat Genet* 39:733-740.

McCoy, A.J., R.W. Grosse-Kunstleve, P.D. Adams, M.D. Winn, L.C. Storoni, and R.J. Read. 2007. Phaser crystallographic software. *J Appl Crystallogr* 40:658-674.

Mulrooney, T.J., A.C. Zhang, Y. Goldgur, J.E. Boudreau, and K.C. Hsu. 2015. KIR3DS1-Specific D0 Domain Polymorphisms Disrupt KIR3DL1 Surface Expression and HLA Binding. *J Immunol*

Norman, P.J., L. Abi-Rached, K. Gendzekhadze, J.A. Hammond, A.K. Moesta, D. Sharma, T. Graef, K.L. McQueen, L.A. Guethlein, C.V. Carrington, D. Chandanayingyong, Y.H. Chang, C. Crespi, G. Saruhan-Direskeneli, K. Hameed, G. Kamkamidze, K.A. Koram, Z. Layrisse, N. Matamoros, J. Mila, M.H. Park, R.M. Pitchappan, D.D. Ramdath, M.Y. Shiau, H.A. Stephens, S. Struik, D. Tyan, D.H. Verity, R.W. Vaughan, R.W. Davis, P.A. Fraser, E.M. Riley, M. Ronaghi, and P. Parham. 2009. Meiotic recombination generates rich diversity in NK cell receptor genes, alleles, and haplotypes. *Genome research* 19:757-769.

Norman, P.J., L. Abi-Rached, K. Gendzekhadze, D. Korbel, M. Gleimer, D. Rowley, D. Bruno, C.V. Carrington, D. Chandanayingyong, Y.H. Chang, C. Crespi, G. Saruhan-Direskeneli, P.A. Fraser, K. Hameed, G. Kamkamidze, K.A. Koram, Z. Layrisse, N. Matamoros, J. Mila, M.H. Park, R.M. Pitchappan, D.D. Ramdath, M.Y. Shiau, H.A. Stephens, S. Struik, D.H. Verity, R.W. Vaughan, D. Tyan, R.W. Davis, E.M. Riley, M. Ronaghi, and P. Parham. 2007. Unusual selection on the KIR3DL1/S1 natural killer cell receptor in Africans. *Nat Genet* 39:1092-1099.

O'Connor, G.M., K.J. Guinan, R.T. Cunningham, D. Middleton, P. Parham, and C.M. Gardiner. 2007. Functional polymorphism of the KIR3DL1/S1 receptor on human NK cells. *J Immunol* 178:235-241.

O'Connor, G.M., J.P. Vivian, J.M. Widjaja, J.S. Bridgeman, E. Gostick, B.A. Lafont, S.K. Anderson, D.A. Price, A.G. Brooks, J. Rossjohn, and D.W. McVicar. 2014. Mutational and Structural Analysis of KIR3DL1 Reveals a Lineage-Defining Allotypic Dimorphism That Impacts Both HLA and Peptide Sensitivity. *J Immunol* 192:2875-2884.

Pan, N., W. Jiang, H. Sun, F. Miao, J. Qiu, H. Jin, J. Xu, Q. Shi, W. Xie, and J. Zhang. 2011. <italic>KIR</italic> and <italic>HLA</italic> Loci Are Associated with Hepatocellular Carcinoma Development in Patients with Hepatitis B Virus Infection: A Case-Control Study. *PLoS ONE* 6:e25682.

Pando, M.J., C.M. Gardiner, M. Gleimer, K.L. McQueen, and P. Parham. 2003. The protein made from a common allele of KIR3DL1 (3DL1*004) is poorly expressed at cell surfaces due to substitution at positions 86 in Ig domain 0 and 182 in Ig domain 1. *J Immunol* 171:6640-6649.

Parham, P., P.J. Norman, L. Abi-Rached, and L.A. Guethlein. 2012. Human-specific evolution of killer cell immunoglobulin-like receptor recognition of major histocompatibility complex class I molecules. *Philos Trans R Soc Lond B Biol Sci* 367:800-811.

Pende, D., S. Marcenaro, M. Falco, S. Martini, M.E. Bernardo, D. Montagna, E. Romeo, C. Cognet, M. Martinetti, R. Maccario, M.C. Mingari, E. Vivier, L. Moretta, F. Locatelli, and A. Moretta. 2009. Anti-leukemia activity of alloreactive NK cells in KIR ligand-mismatched haploidentical HSCT for pediatric patients: evaluation of the functional role of activating KIR and redefinition of inhibitory KIR specificity. *Blood* 113:3119-3129.

Petrie, E.J., C.S. Clements, J. Lin, L.C. Sullivan, D. Johnson, T. Huyton, A. Heroux, H.L. Hoare, T. Beddoe, H.H. Reid, M.C. Wilce, A.G. Brooks, and J. Rossjohn. 2008. CD94-NKG2A recognition of human leukocyte antigen (HLA)-E bound to an HLA class I leader sequence. *J Exp Med* 205:725-735.

Robinson, J., J.A. Halliwell, J.D. Hayhurst, P. Flicek, P. Parham, and S.G. Marsh. 2015. The IPD and IMGT/HLA database: allele variant databases. *Nucleic Acids Res* 43:D423-431.

Rojo, S., N. Wagtmann, and E.O. Long. 1997. Binding of a soluble p70 killer cell inhibitory receptor to HLA-B*5101: requirement for all three p70 immunoglobulin domains. *European journal of immunology* 27:568-571.

Saunders, P.M., J.P. Vivian, N. Baschuk, T. Beddoe, J. Widjaja, G.M. O'Connor, C. Hitchen, P. Pymm, D.M. Andrews, S. Gras, D.W. McVicar, J. Rossjohn, and A.G. Brooks. 2015. The Interaction of KIR3DL1*001 with HLA Class I Molecules Is Dependent upon Molecular Microarchitecture within the Bw4 Epitope. *J Immunol* 194:781-789.

Sharma, D., K. Bastard, L.A. Guethlein, P.J. Norman, N. Yawata, M. Yawata, M. Pando, H. Thananchai, T. Dong, S. Rowland-Jones, F.M. Brodsky, and P. Parham. 2009. Dimorphic motifs in D0 and D1+D2 domains of killer cell Ig-like receptor 3DL1 combine to form receptors with high, moderate, and no avidity for the complex of a peptide derived from HIV and HLA-A*2402. *J Immunol* 183:4569-4582.

Solberg, O.D., S.J. Mack, A.K. Lancaster, R.M. Single, Y. Tsai, A. Sanchez-Mazas, and G. Thomson. 2008. Balancing selection and heterogeneity across the classical human leukocyte antigen loci: a meta-analytic review of 497 population studies. *Human immunology* 69:443-464.

Stifter, S.A., J.A. Gould, N.E. Mangan, H.H. Reid, J. Rossjohn, P.J. Hertzog, and N.A. de Weerd. 2014. Purification and biological characterization of soluble, recombinant mouse IFNbeta expressed in insect cells. *Protein expression and purification* 94:7-14.

Taner, S.B., M.J. Pando, A. Roberts, J. Schellekens, S.G. Marsh, K.J. Malmberg, P. Parham, and F.M. Brodsky. 2011. Interactions of NK cell receptor KIR3DL1*004 with chaperones and conformation-specific antibody reveal a functional folded state as well as predominant intracellular retention. *J Immunol* 186:62-72.

Thananchai, H., G. Gillespie, M.P. Martin, A. Bashirova, N. Yawata, M. Yawata, P. Easterbrook, D.W. McVicar, K. Maenaka, P. Parham, M. Carrington, T. Dong, and S. Rowland-Jones. 2007. Cutting Edge: Allele-specific and peptide-dependent interactions between KIR3DL1 and HLA-A and HLA-B. *J Immunol* 178:33-37.

Tsutsui, Y., L. Liu, A. Gershenson, and P.L. Wintrode. 2006. The conformational dynamics of a metastable serpin studied by hydrogen exchange and mass spectrometry. *Biochemistry* 45:6561-6569.

Vivian, J.P., R.C. Duncan, R. Berry, G.M. O'Connor, H.H. Reid, T. Beddoe, S. Gras, P.M. Saunders, M.A. Olshina, J.M. Widjaja, C.M. Harpur, J. Lin, S.M. Maloveste, D.A. Price, B.A. Lafont, D.W. McVicar, C.S. Clements, A.G. Brooks, and J. Rossjohn. 2011. Killer cell immunoglobulin-like receptor 3DL1-mediated recognition of human leukocyte antigen B. *Nature* 479:401-405.

Yawata, M., N. Yawata, M. Draghi, A.-M. Little, F. Partheniou, and P. Parham. 2006a. Roles for HLA and KIR polymorphisms in natural killer cell repertoire selection and modulation of effector function. *The Journal of Experimental Medicine* 203:633-645.

Yawata, M., N. Yawata, M. Draghi, A.M. Little, F. Partheniou, and P. Parham. 2006b. Roles for HLA and KIR polymorphisms in natural killer cell repertoire selection and modulation of effector function. *The Journal of experimental medicine* 203:633-645.

FIGURE LEGENDS

Figure 1: *Inhibition of KIR3DL1$^+$ NK cells varies with HLA-Bw4 expressing targets.* A) Amino acid sequences across residues 77-83 of transfected HLA class I molecules. B) The surface expression of transfected HLA class I molecules was confirmed by staining with W6/32 (grey histogram) or anti-Bw4 (black histogram) mAbs followed by anti-mouse IgG-FITC. Filled grey histograms represent background staining with secondary antibody alone. C and D) KIR3DL1$^+$ NK cells were sorted from eight donors and expanded with IL-2. Equal numbers of KIR3DL1$^+$ NK cells and 221 transfected target cells were cultured with the addition of anti-CD107a for four hours in the presence of monensin. CD107a expression was then examined by flow cytometry, gating on CD56$^+$/NKB1$^+$ cells. (C). Representative flow cytometric plots showing CD107a expression. Values indicate % of cells expressing CD107a. (D) Normalised CD107a expression following coculture of KIR3DL1+ NK cells with transfected or parental 221 cells where the response to untransfected 221 cells was adjusted to 100%. Data are pooled from 6 independent experiments. E) The mean fluorescence intensity (MFI) of W6/32 versus the MFI of subsequent CD107a expression is plotted for each 221 transfectant for a representative donor.

Figure 2: *Tetramers of each KIR3DL1 allomorph display distinct binding preferences to HLA-I coated beads.*

(A) The fluorescent values for the top 25 HLA alleles binding to each KIR3DL1 allotype in the HLA class I bead assay are shown as normalized values for KIR3DL1*015, KIR3DL1*001 and KIR3DL1*015. HLA are categorized by percentage maximum binding with 100-75% maximum binding (red), 75-50% maximum binding (pink), 50-25% maximum binding (grey) and 25-0% binding (teal). (B) KIR3DL1 allotype recognition for all HLA Bw4 containing allomorphs present on the bead assay are plotted and separated by dimorphism at position 80 (80I and 80T). Binding values are given as i. normalized binding and ii. mean fluorescent intensities (MFI). Significant differences between Bw4 80I and Bw4 80T subtype recognition as measured by independent multiple T tests are shown with an asterisk. (C) HLA class I alleles on the bead assay are ranked by recognition of KIR3DL1*015, the top 28 alleles are depicted with comparison of rank and binding values for these alleles to those for the KIR3DL1*001 and *005 allotypes. HLA are shown by i. rank and ii. percentage of highest binding allele. All data represent mean values from three independent experiments. Error bars depict one Standard Deviation from the mean value.

Figure 3: *KIR3DL1 molecules of different lineages functionally discriminate between HLA-Bw4 ligands* (A) The polymorphic residues found in KIR3DL1*015, *002, *001, *009, *005 and *004

(and the KIR3DS1 lineage) are shown, with additional residues of variance also noted (list is not exhaustive). B) KIR3DL1^{+} NKG2A^{-} cells were sorted and cloned from three healthy volunteers of known KIR3DL1 allotype (LM *001; RM *002/*00501; BC *00501). Cloned NK cells were then incubated with ^{51}Cr-labeled 221 transfectants at the indicated E:T ratios in the presence or absence of anti-KIR3DL1/S1 (Z27). Data shown is average cytotoxicity±SEM where the response to untransfected 221 cells was adjusted to 100%, based on the maximal cytotoxicity observed in the presence of parental 221 targets and in the absence of Z27. The number of clones individually assessed at the given ratios is noted in brackets. Data shown is pooled from 6 independent experiments C) PBMC were isolated from unknown donors, KIR3DL1^{+} cells sorted and cloned and the KIR3DL1 alleles sequenced. Expanded NK clones were incubated with 221 transfectants at a 1:1 ratio with the addition of a CD94 specific blocking mAb Y9, along with anti-CD107a, followed by monensin. After four hours incubation, cells were stained for CD56 and KIR3DL1, and CD107a expression assessed by flow cytometry. Experiments were performed once for each clone with the CD107a expression normalised to the maximal CD107a expression observed following coculture in the presence of untransfected 221 cells. Plot shows average CD107a expression ± SEM with the number of clones assessed noted in brackets. Data were pooled from 5 independent experiments.

Figure 4: *Structural comparison of KIR3DL1 allomorphs in complex with HLA-B*57:01.* (A) The location of the polymorphic differences between KIR3DL1*001, *005 and *015 mapped on to the structure of KIR3DL1*005 in complex with HLA-B*57:01. (B) Close-up view of KIR3DL1*005 in complex with HLA-B*57:01. Highlighted regions are the Bw4 motif on the α1 helix (yellow sticks) and the primary contacts between the KIR3DL1 (cyan) and HLA-B*57:01 (yellow sticks). (C and D) Docking of KIR3DL1 allotypes onto HLA-B*57:01-LF9. The axes of inertia of each of the KIR3DL1 domains are shown as rods. KIR3DL1*001 coloured orange, *005 coloured blue and *015 coloured yellow. The hinge-angles between the domains are shown in (C) and the crossing angles of the domains in (D).

Figure 5: *Structural details underpinning the differences between KIR3DL1 allomorphs in complex with HLA-B*57:01.* (A) Two conformations of the C-C′ loop of KIR3DL1 are present in complex with HLA-B*57:01. The loop as observed in the KIR3DL1*001 complex is coloured orange and the conformation as observed in *005/*015 is coloured blue. (B and C) The structural consequences surrounding the site of the KIR3DL1 W283L dimorphism at the D1/D2 interface. The conformation as observed in KIR3DL1*001/*015 is shown in panel (B). The conformation as observed in KIR3DL1*005 is shown in panel (C). (D) Subtle differences at positions Met165 and His278

differentiate the binding of KIR3DL1*001 and *005. The conformation as observed in KIR3DL1*001/*015 is coloured orange whilst the conformation as observed in *005 is coloured blue.

Figure 6. *KIR3DL1*005 displays greater molecular mobility across three ligand-binding loops.*
(A-F) Hydrogen-deuterium exchange of peptidic fragments from KIR3DL1. Representative *m/z* spectra of each peptidic fragment after 30 s are shown for each KIR3DL1*015 (yellow), *001 (orange) and *005 (blue) and at time 0 s (magenta). Bar graphs show the extent of deuterium exchange for each KIR3DL1 allomorph plotted at time points 0, 10 and 30 s. Panels A-C show peptidic fragments derived from the KIR3DL1 D1 and D1/D2 linker. Panels D-F show peptidic fragments derived from the KIR3DL1 D2. Data from three independent experiments (each time point in triplicate). Error bars depict SEM.

Table 1: Refinements statistics for KIR3DL1*005 and KIR3DL1*015

	KIR3DL1*005-HLA-B*57:01-LF9	KIR3DL1*015-HLA-B*57:01-LF9
Data collection statistics		
Temperature (K)	100	100
X-ray source	MX2 Australian synchrotron	MX2 Australian synchrotron
Space group	*P*1	*P*1
Cell Dimensions	*a* = 51.6, *b*= 61.3, *c*=66.4 α= 95.2, β= 100.2, γ=108.2	*a* = 51.6, *b*= 61.1, *c*= 65.1, α= 95.6, β= 98.5 γ= 108.6
Resolution Å	50 – 2.30 (2.42 – 2.30)	50 – 2.5 (2.64 – 2.50)
Total no. observations	139081 (20784)	99352 (14846)
No. unique observations	30955 (4571)	23125 (3419)
Multiplicity	4.5 (4.5)	4.3 (4.3)
Data completeness (%)	92.9 (95.0)	90.7 (91.5)
$1/\sigma_I$	6.9 (3.6)	7.3 (3.7)
R_{merge}[1]	0.144 (0.421)	0.188 (0.897)
Refinement statistics		
Non-hydrogen atoms		
Protein	5260	5294
Water	230	148
R_{factor}[2]	0.20	0.18
R_{free}[2]	0.25	0.23
r.m.s.d. from ideality		
Bond lengths (Å)	0.003	0.005
Bond angles (°)	0.702	0.874
Ramachandran plot		
Favoured regions (%)	95.0	95.4
Allowed regions (%)	5.0	4.6
B-factors (Å^2)		
Average main chain	34	32
Average side chain	38	37
Average water	38	36

[1] $R_{merge} = \sum_{hkl} \sum_j |I_{hkl,j} - < I_{hkl} > | / \sum_{hkl} \sum_j I_{hkl,j}$.

[2] $R_{factor} = \sum_{hkl} ||F_o| - |F_c|| / \sum_{hkl} |F_o|$ for all data excluding the 5% that comprised the R_{free} used for cross-validation.

Figure 1

A

	HLA residue						
	77	78	79	80	81	82	83
B*57:01	N	L	R	I	A	L	R
B*58:01	-	-	-	-	-	-	-
A*24:02	-	-	-	-	-	-	-
B*44:05	-	-	-	T	-	-	-
B*27:05	D	-	-	T	L	-	-
B*08:01	S	-	-	N	L	R	G

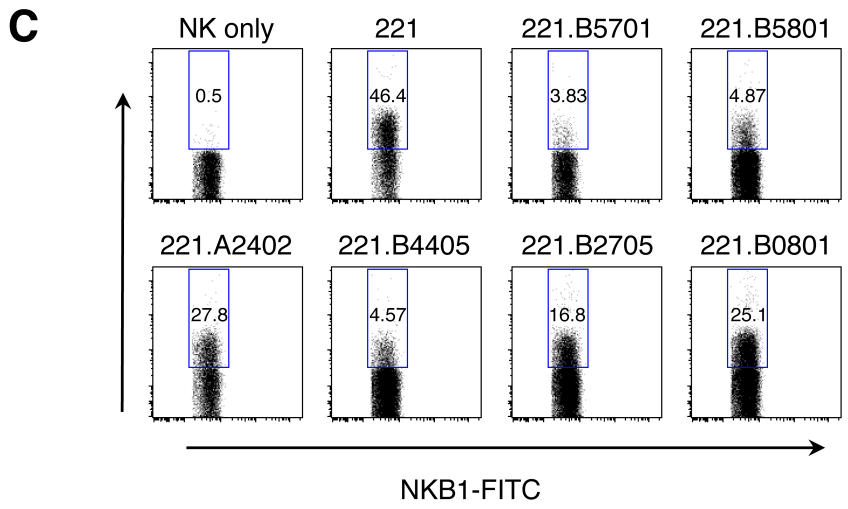

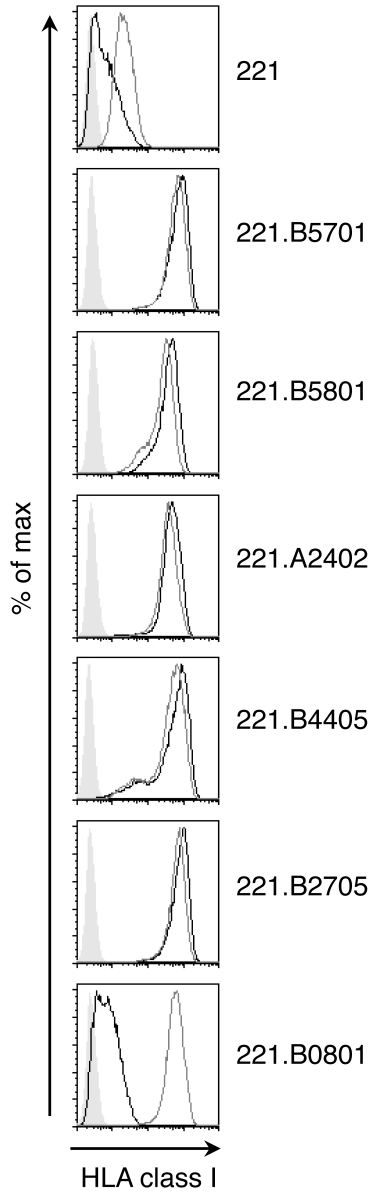

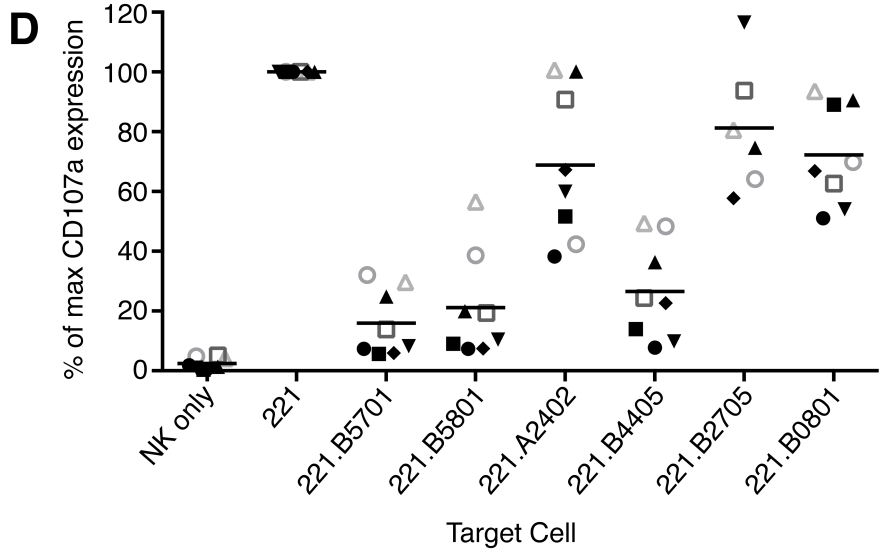

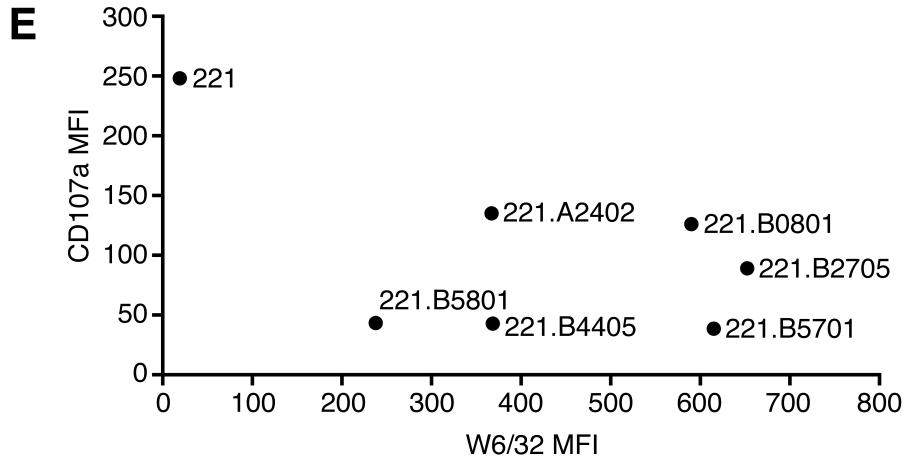

Figure 2

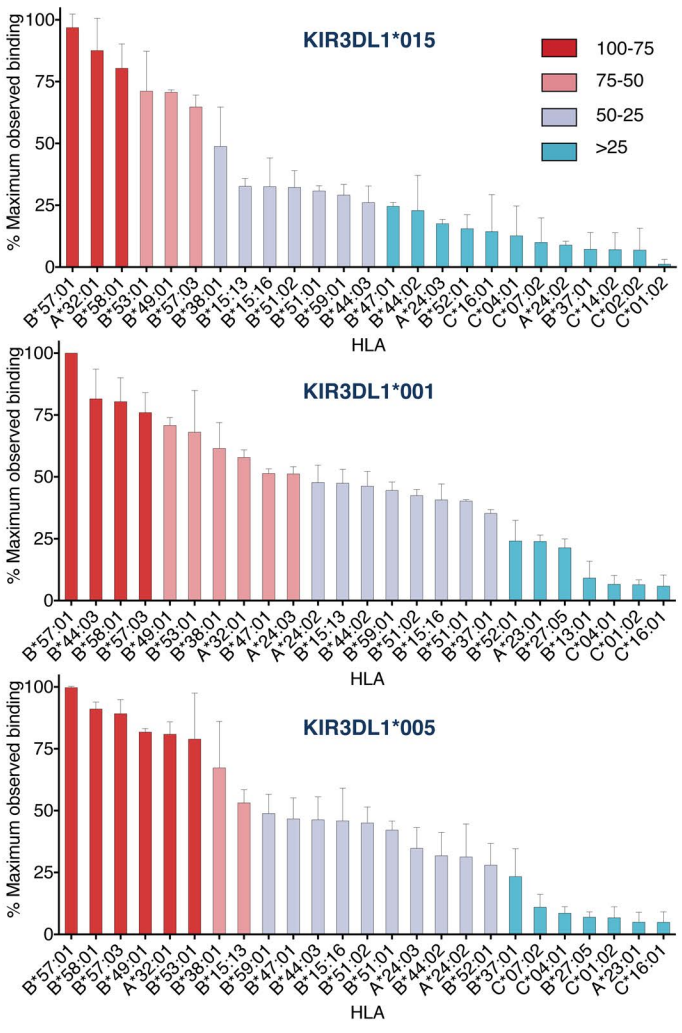

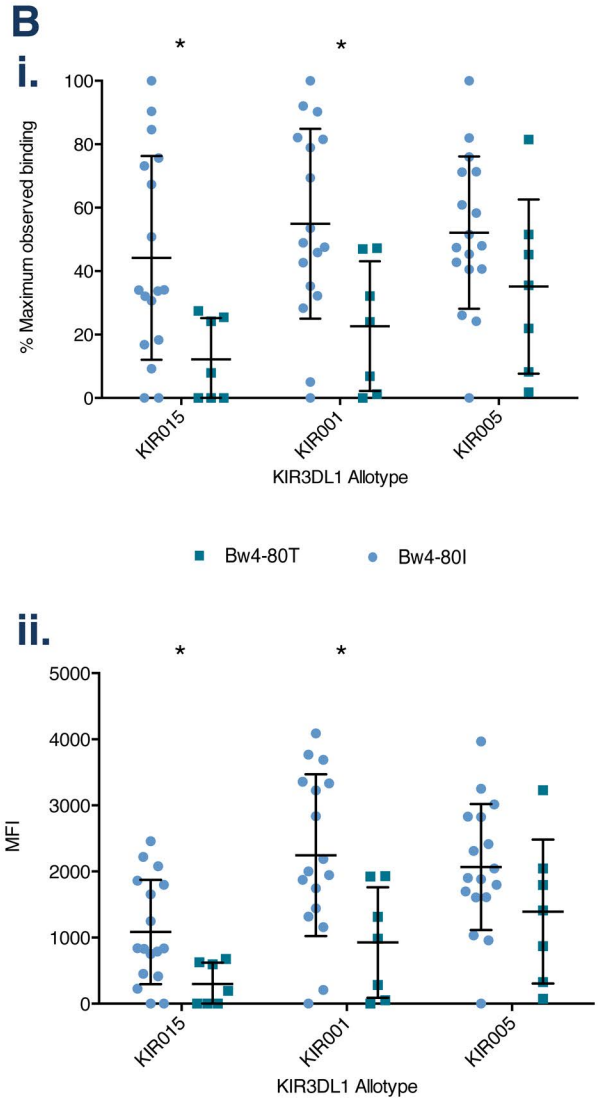

C i.

HLA	Bw Subtype	KIR015	KIR001	KIR005
B*57:01	Bw4 80I	96.8	99.7	100
A*32:01	Bw4 80I	87.6	80.9	57.9
B*58:01	Bw4 80I	80.4	91.1	80.4
B*53:01	Bw4 80I	71.2	78.9	68.1
B*49:01	Bw4 80I	70.7	81.8	70.8
B*57:03	Bw4 80I	64.8	89.1	76.0
B*38:01	Bw4 80I	48.8	67.3	61.5
B*15:13	Bw4 80I	32.6	53.1	47.4
B*15:16	Bw4 80I	32.5	45.9	40.7
B*51:02	Bw4 80I	32.2	45.0	42.4
B*51:01	Bw4 80I	30.8	42.1	40.2
B*59:01	Bw4 80I	29.1	48.9	44.5
B*44:03	Bw4 80T	26.1	46.3	81.5
B*47:01	Bw4 80T	24.5	46.6	51.4
B*44:02	Bw4 80T	22.9	31.8	46.2
A*24:03	Bw4 80I	17.6	34.8	51.2
B*52:01	Bw4 80I	15.5	28.0	24.1
C*16:01	C1 N	14.4	4.87	5.84
C*04:01	C2 K	12.7	8.55	6.59
C*07:02	C1 N	10.0	11.0	5.62
A*24:02	Bw4 80I	8.91	31.2	47.7
B*37:01	Bw4 80T	7.24	23.4	35.2
C*14:02	C1 N	7.06	4.42	5.45
C*02:02	C2 K	6.90	4.13	4.17
C*01:02	C1 N	1.14	6.72	6.43
A*23:01	Bw4 80I	0.00	4.95	23.9
B*27:05	Bw4 80T	0.00	6.92	21.3
B*13:01	Bw4 80T	0.00	0.00	9.12

ii.

HLA	Bw Subtype	KIR015	KIR001	KIR005
B*57:01	Bw4 80I	1	1	1
A*32:01	Bw4 80I	2	5	8
B*58:01	Bw4 80I	3	2	3
B*53:01	Bw4 80I	4	6	6
B*49:01	Bw4 80I	5	4	5
B*57:03	Bw4 80I	6	3	4
B*38:01	Bw4 80I	7	7	7
B*15:13	Bw4 80I	8	8	12
B*15:16	Bw4 80I	9	12	16
B*51:02	Bw4 80I	10	13	15
B*51:01	Bw4 80I	11	14	17
B*59:01	Bw4 80I	12	9	14
B*44:03	Bw4 80T	13	11	2
B*47:01	Bw4 80T	14	10	9
B*44:02	Bw4 80T	15	16	13
A*24:03	Bw4 80I	16	15	10
B*52:01	Bw4 80I	17	18	19
C*16:01	C1 N	18	25	25
C*04:01	C2 K	19	21	23
C*07:02	C1 N	20	20	26
A*24:02	Bw4 80I	21	17	11
B*37:01	Bw4 80T	22	19	18
C*14:02	C1 N	23	26	27
C*02:02	C2 K	24	27	28
C*01:02	C1 N	25	23	24
A*23:01	Bw4 80I	N/A	24	20
B*27:05	Bw4 80T	N/A	22	21
B*13:01	Bw4 80T	N/A	N/A	22

Figure 3

A

KIR3DL1 residue

	D0											D1						D2				TM-tail		
3DL1	-20	-9	2	18	31	44	47	54	58	75	86	92	138	141	145	163	166	182	199	238	256	283	320	343	373
*015	L	F	V	V	R	R	V	L	S	R	S	V	G	K	R	P	L	P	P	G	Q	W	I	C	E
*002	-	-	-	-	-	-	-	-	-	-	-	-	-	-	-	-	-	-	-	R	-	-	-	-	-
*001	S	L	M	-	-	-	I	I	-	-	-	-	-	-	-	-	-	-	-	-	-	-	-	-	-
*009	S	L	M	-	-	-	-	I	G	-	-	M	-	-	-	-	-	-	-	-	-	-	-	-	-
*005	S	L	M	-	-	-	I	I	-	-	-	-	-	-	-	-	-	S	-	-	-	L	-	-	-
*004	S	L	M	-	H	G	I	I	-	-	L	-	-	-	-	-	-	S	-	-	-	L	V	Y	Q
3DS1																									
*013	-	L	M	-	-	-	-	I	G	-	-	M		-	-	S	R	-	L	-	-	-			

B

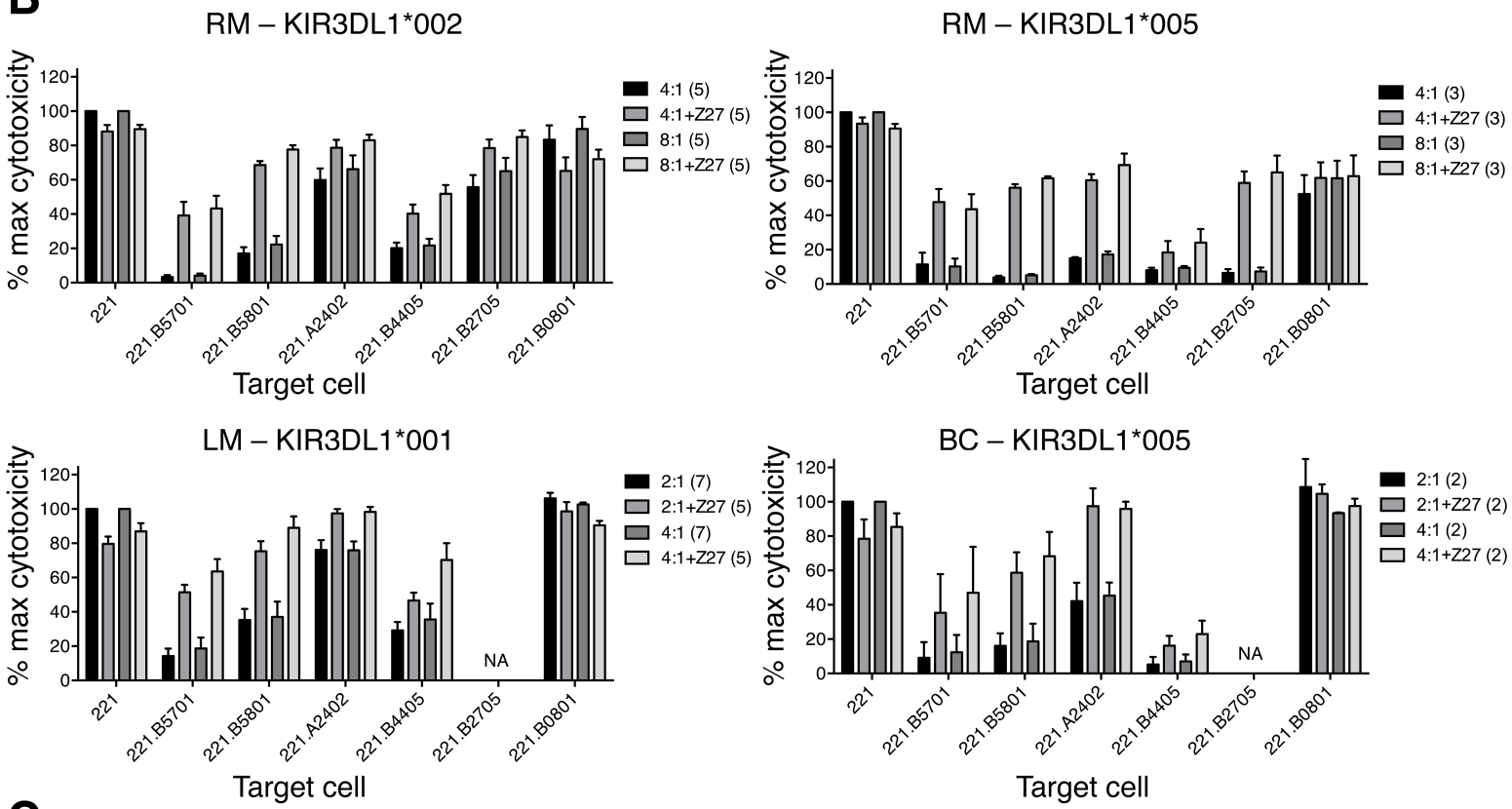

C

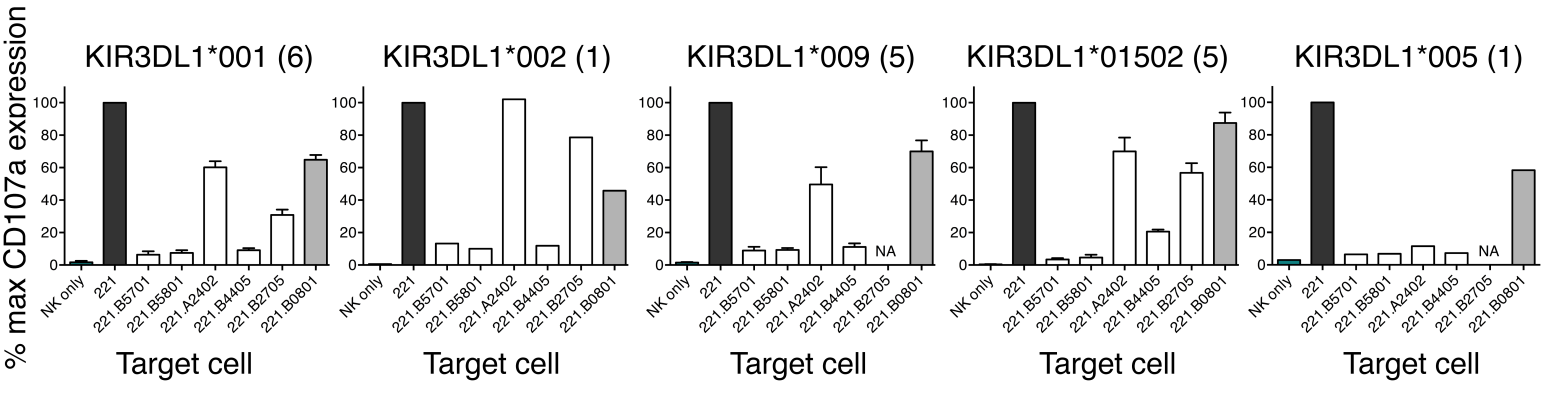

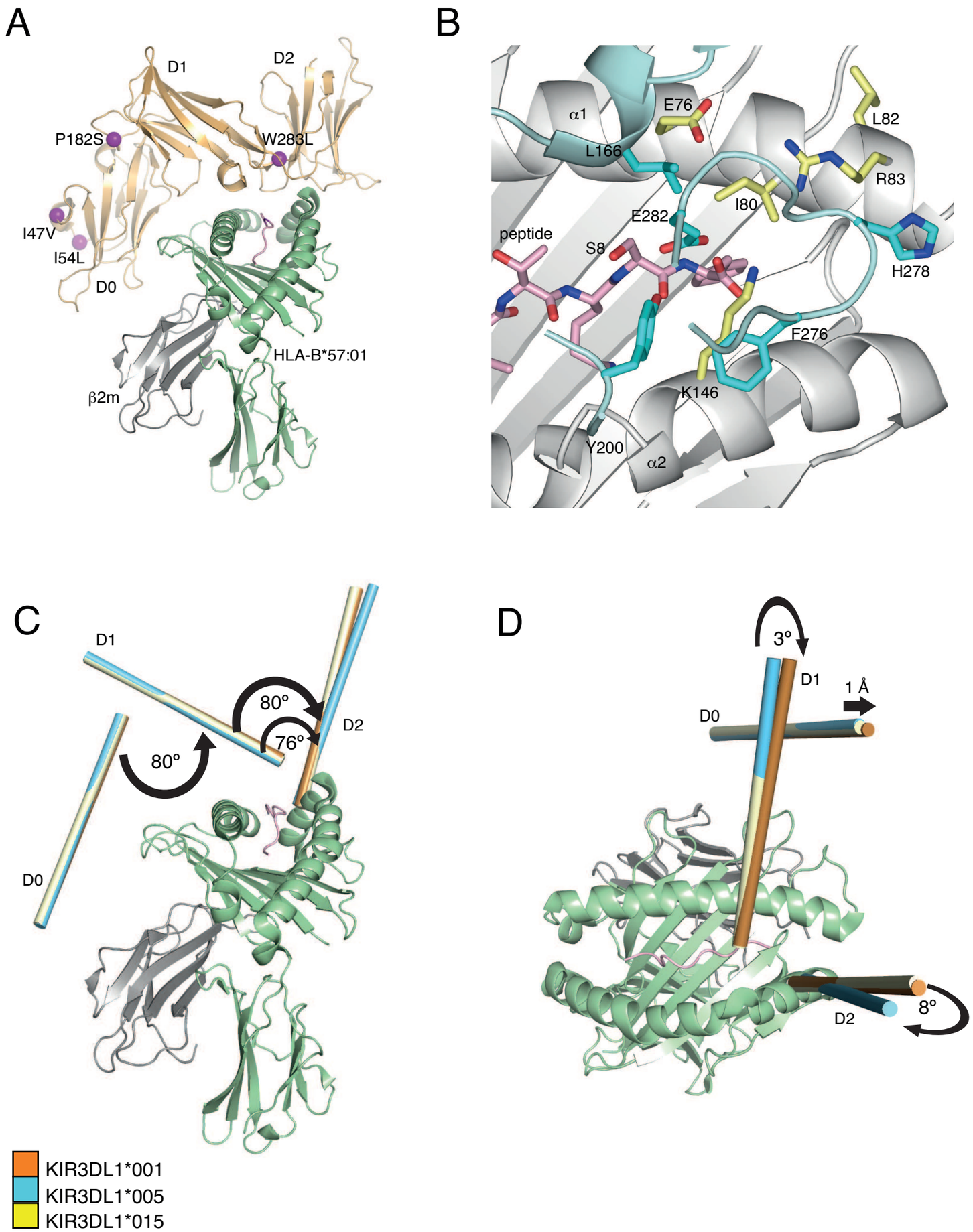
A
D1
D2
P182S
W283L
I47V
I54L
D0
HLA-B*57:01
β2m
B
α1
E76
L82
L166
R83
I80
E282
peptide
S8
H278
F276
K146
Y200
α2
C
D1
80°
D2
76°
80°
D0
KIR3DL1*001
KIR3DL1*005
KIR3DL1*015
D
3°
D1
1 Å
D0
D2
8°

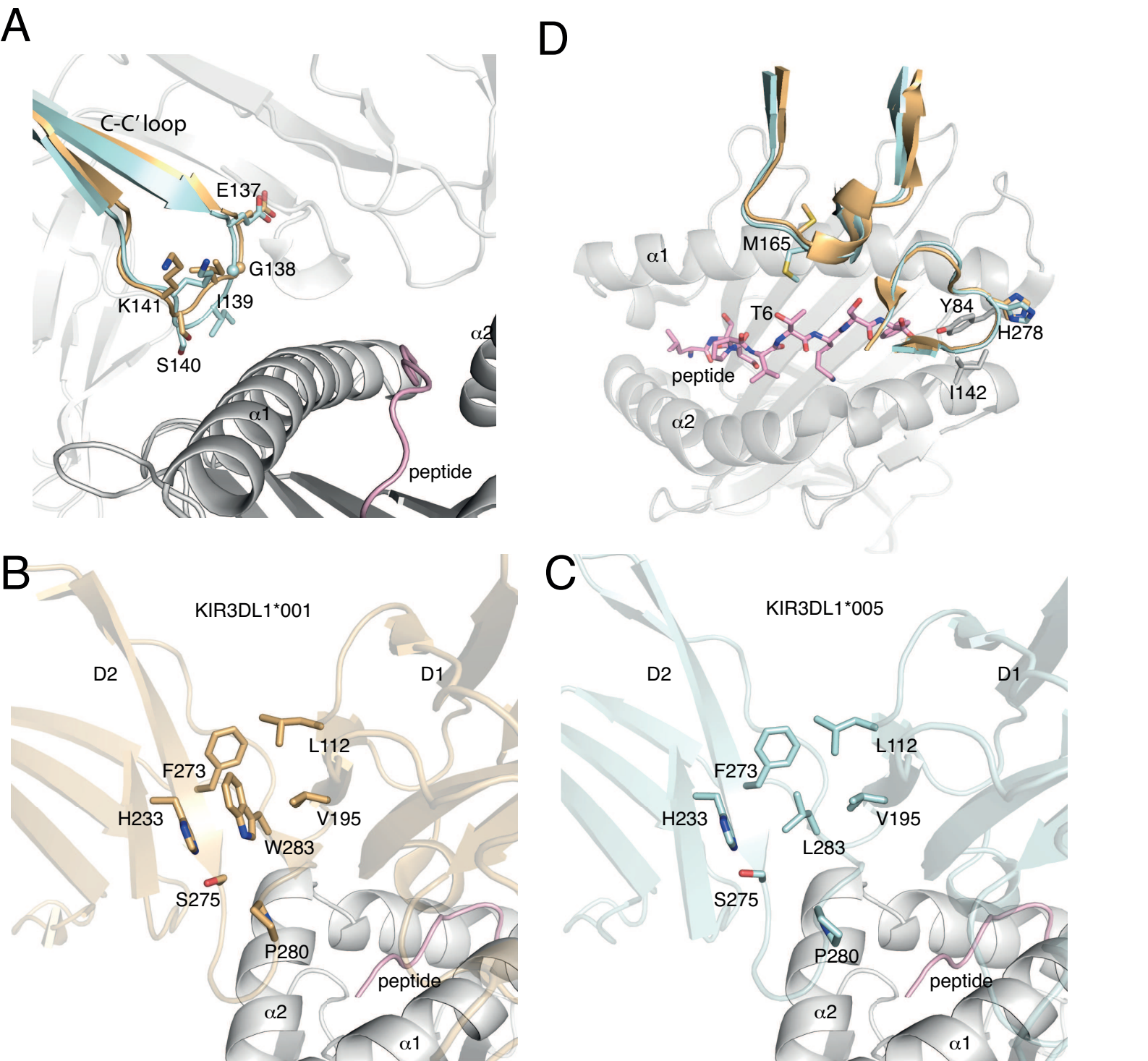
A
C-C′ loop
E137
G138
K141
I139
S140
α2
α1
peptide
D
α1
M165
T6
Y84
H278
peptide
I142
α2
B
KIR3DL1*001
D2
D1
L112
F273
H233
V195
W283
S275
P280
peptide
α2
α1
C
KIR3DL1*005
D2
D1
L112
F273
H233
V195
L283
S275
P280
peptide
α2
α1

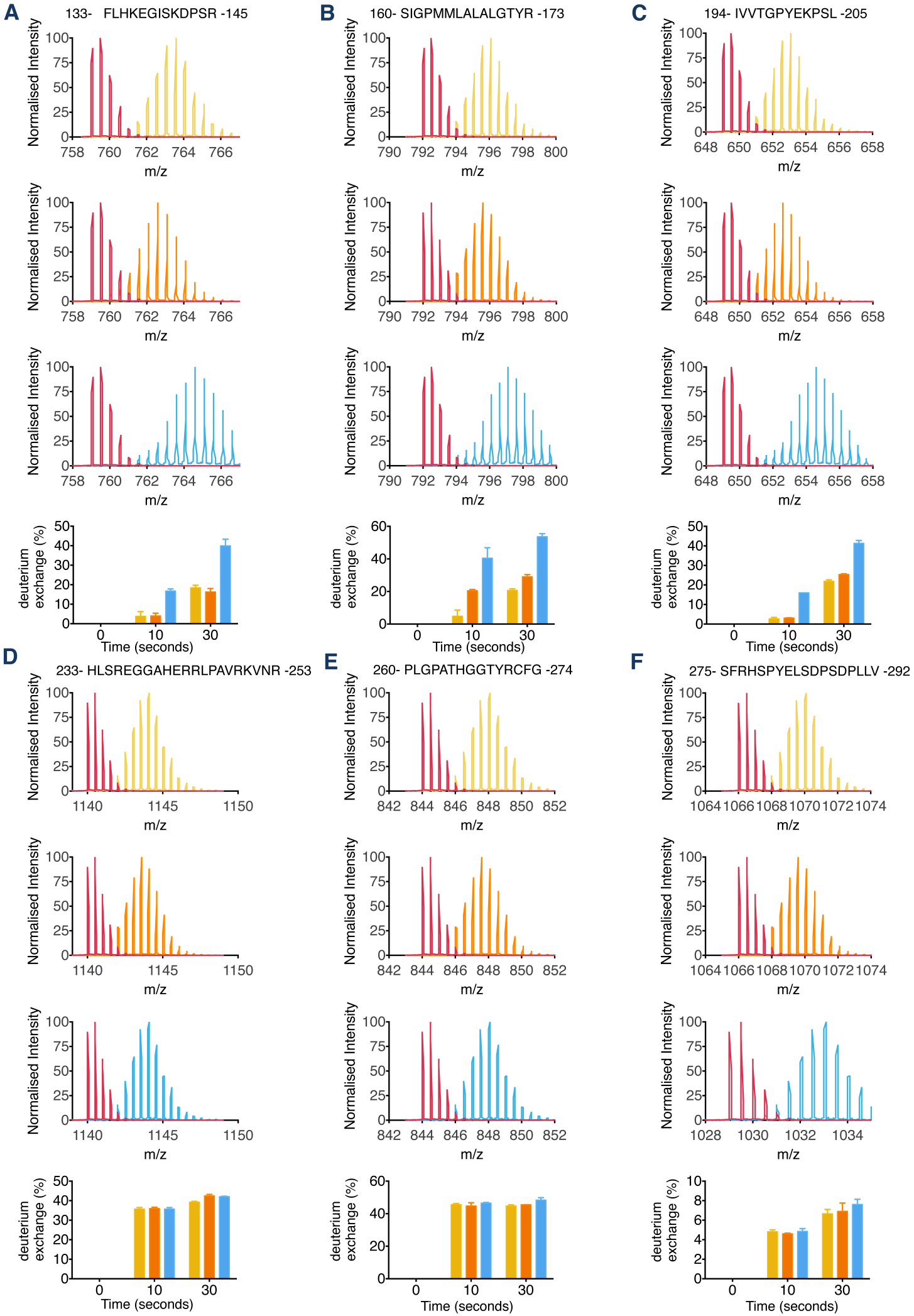
A
133- FLHKEGISKDPSR -145
B
160- SIGPMMLALALGTYR -173
C
194- IVVTGPYEKPSL -205
D
233- HLSREGGAHERRLPAVRKVNR -253
E
260- PLGPATHGGTYRCFG -274
F
275- SFRHSPYELSDPSDPLLV -292
Normalised Intensity
m/z
deuterium exchange (%)
Time (seconds)